Article

Cell Host & Microbe

Chlamydia repurposes the actin-binding protein EPS8 to disassemble epithelial tight junctions and promote infection

Graphical abstract

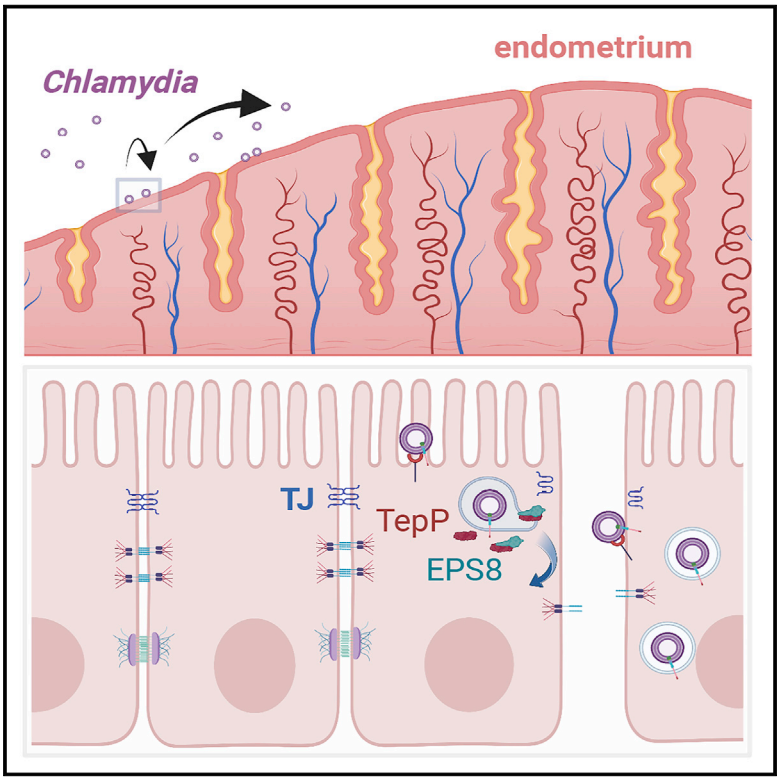

Authors

Lee Dolat, Victoria K. Carpenter, Yi-Shan Chen, Michitaka Suzuki, Erin P. Smith, Ozge Kuddar, Raphael H. Valdivia

Correspondence

raphael.valdivia@duke.edu

In brief

Dolat et al. show that the obligate intracellular pathogen, *Chlamydia trachomatis*, disrupts epithelial tight junctions to promote infection. The authors identify a role for the *C. trachomatis*-secreted effector TepP in repurposing the host actin-binding protein EPS8 to dismantle tight junctions and promote the invasion of polarized epithelia.

Highlights

- *C. trachomatis* transiently disrupts epithelial tight junctions
- The effector TepP interacts with EPS8 and recruits it to nascent inclusions
- TepP repurposes EPS8 to disrupt tight junctions and promote *Chlamydia* entry
- TepP and EPS8 promote infection in mouse models of *Chlamydia* infection

Dolat et al., 2022, Cell Host & Microbe *30*, 1–16
December 14, 2022
https://doi.org/10.1016/j.chom.2022.10.013

CellPress

Cell Host & Microbe

CellPress

Article

Chlamydia repurposes the actin-binding protein EPS8 to disassemble epithelial tight junctions and promote infection

Lee Dolat,[1] Victoria K. Carpenter,[1] Yi-Shan Chen,[1] Michitaka Suzuki,[1] Erin P. Smith,[1] Ozge Kuddar,[1] and Raphael H. Valdivia[1,2,*]

[1]Department of Molecular Genetics and Microbiology, Duke University Medical Center, Durham, NC 27710, USA

[2]Lead contact

*Correspondence: raphael.valdivia@duke.edu

https://doi.org/10.1016/j.chom.2022.10.013

SUMMARY

Invasive microbial pathogens often disrupt epithelial barriers, yet the mechanisms used to dismantle tight junctions are poorly understood. Here, we show that the obligate pathogen *Chlamydia trachomatis* uses the effector protein TepP to transiently disassemble tight junctions early during infection. TepP alters the tyrosine phosphorylation status of host proteins involved in cytoskeletal regulation, including the filamentous actin-binding protein EPS8. We determined that TepP and EPS8 are necessary and sufficient to remodel tight junctions and that the ensuing disruption of epithelial barrier function promotes secondary invasion events. The genetic deletion of EPS8 renders epithelial cells and endometrial organoids resistant to TepP-mediated tight junction remodeling. Finally, TepP and EPS8 promote infection in murine models of infections, with TepP mutants displaying defects in ascension to the upper genital tract. These findings reveal a non-canonical function of EPS8 in the disassembly of epithelial junctions and an important role for *Chlamydia* pathogenesis.

INTRODUCTION

Chlamydia trachomatis is an obligate intracellular pathogen responsible for the majority of sexually transmitted bacterial infections and remains the leading cause of preventable infectious blindness.[1] In urogenital *C. trachomatis* infection, the ensuing inflammatory response drives the manifestation of disease including pelvic inflammatory diseases, tubal scarring, and infertility.[2] *C. trachomatis* targets polarized columnar epithelial cells in the cervical transition zones and upper female reproductive tract. Epithelial polarity is spatially coupled to cell-cell contacts, including tight junctions, adherens junctions, and desmosomes.[3] Apical tight junctions maintain epithelial polarity while gating the movement of solutes and ions through the paracellular space.[4] Bacterial and viral pathogens can disrupt epithelial organization and polarity by directly and indirectly targeting tight junctions to promote microbial invasion or transit to the underlying tissue.[5,6] In polarized epithelial infection models, *C. trachomatis* disrupts epithelial cell-cell junctions,[7,8] but the mechanism mediating this disruption is unknown.

Chlamydiae exhibit a biphasic life cycle—the extracellular and infectious elementary body (EB) and the intracellular, replication competent reticulate body (RB).[9] The EB form binds epithelial plasma membrane proteoglycans (e.g., heparan sulfate) and receptors, such as integrin B1, ephrin receptor A2, epidermal growth factor receptor (EGFR), and platelet-derived growth factor receptor beta (PDGFR2).[10–14] Effector proteins are translocated into target cells via a Type III secretion (T3S) system to stimulate actin assembly and the formation of a membrane-bound pathogen-containing vacuole termed an "inclusion" (reviewed in Elwell et al.[15]). Early inclusions migrate to the peri-nuclear region where the bacteria differentiate into the replicative RB form.[16,17] Eventually, RBs asynchronously differentiate back into the EB form. At the end of the infectious cycle, the inclusion is extruded extracellularly or EBs are released after lysis of the host cell.[18]

A subset of T3S effectors is pre-engaged with the T3S chaperone Slc1 to regulate their secretion during the invasion of epithelial cells.[19,20] Two effectors directly rearrange the actin cytoskeleton to promote EB entry and inclusion formation—translocated actin phospho-protein (TarP) and translocated membrane-associated effector A (TmeA).[21,22] These effectors converge on the host Arp2/3 actin nucleation complex, and mutant strains in either effector exhibit a reduced invasion of epithelial cells.[23,24] In addition, TarP can activate the Arp2/3 complex by promoting interactions with the guanine nucleotide-exchange factor Rac1.[25] Following the secretion of TarP, the effector translocated early phospho-protein (TepP) is delivered and phosphorylated by Src kinases.[20] TepP is the most abundant effector in the EB form and interacts with the Crk adaptor proteins (Crk I/II, CrkL) and the PI3K complex, which stimulates the formation of $PI(3,4,5)P_3$ on the inclusion membrane.[26,27] TepP also regulates the expression of immunity-related genes during early infection[20] and dampens the recruitment of neutrophils in an *ex vivo* endometrial organoid infection model.[7]

Please cite this article in press as: Dolat et al., *Chlamydia* repurposes the actin-binding protein EPS8 to disassemble epithelial tight junctions and promote infection, Cell Host & Microbe (2022), https://doi.org/10.1016/j.chom.2022.10.013

The phosphorylation of effectors can impact function and activation of signaling events that promote infection and evade innate immune responses.[28] For example, Tyr phosphorylation of the Enteropathogenic *Escherichia coli* effector Tir is required for its interaction with the host adaptor protein Nck, actin assembly, and pedestal formation.[29] Similarly, Tyr phosphorylation of the *Helicobacter pylori* effector CagA regulates its interaction with the SHP2 phosphatase and promotes the elongation of gastric epithelial cells.[30] To modulate the inflammatory state of infected cells, Tyr phosphorylation of the *Bartonella henselae* effector BepD stimulate STAT3 activation and the production of anti-inflammatory cytokines.[31] The effect of TepP phosphorylation, however, is less clear. Although TepP phosphorylation promotes interactions with Crk *in vitro*,[20] Src-mediated phosphorylation is not required for the recruitment of Crk or PI3K to nascent inclusions.[26] Nonetheless, the Tyr phosphorylation of multiple epithelial proteins is TepP-dependent, but their identity is unknown.[20]

Here, we find that TepP directly engages the host epidermal growth factor receptor pathway substrate 8 (EPS8) to alter epithelial cell shape and disrupt tight junctions. EPS8, an actin-capping and bundling protein, normally regulates the assembly and stability of actin-based structures such as stereocilia, filopodia, and microvilli.[32–34] TepP recruits EPS8 to nascent inclusions, triggering the disassembly of epithelial cell-cell junctions, loss of transepithelial electrical resistance (TEER), and cell dispersion. *Chlamydia* then exploits TepP-dependent cell-cell junction breakdown to promote the entry of additional infectious units, presumably by enabling bacterial access to basolateral receptors. The TepP and EPS8-interaction-dependent processes are required for optimal infection of the upper genital tract. These results uncovered an alternative mechanism for *Chlamydia* invasion of cells and details how a bacterial effector can repurpose the function of a cytoskeletal regulatory protein to perform non-canonical activities that enhance infection.

RESULTS

The *C. trachomatis* effector TepP disrupts epithelial tight junctions and promotes cell dispersion

We observed that polarized human endocervical epithelial cells (A2ENs) infected with *Chlamydia trachomatis* strain LGV-L2 (CTL2) transiently dispersed (Figure 1A). The organization of tight junction proteins showed that the nascent inclusion recruits the scaffolding protein, ZO-1 (Figure 1B), which correlated with a transient (<6h) loss of epithelial barrier function as measured by TEER (Figure 1C). Live imaging of A2EN cells infected with *C. trachomatis* indicated a dynamic reorganization of the epithelial monolayer and disruption to cell-cell contacts (Figure 1D; Video S1). This dispersion phenotype was conserved among *C. trachomatis* serovars as infection with urogenital *C. trachomatis* serovars also disrupted barrier function (Figure 1E).

To identify effectors that mediate this early disruption of tight junctions, we infected polarized A2EN cells with *C. trachomatis* mutants defective for Slc1-chaperoned early effectors and measured the degree of epithelial cell dispersion after 1 h. A strain lacking the effector TepP completely abrogated cell dispersion (Figures 1F–1H), which was rescued upon complementation with TepP expression from a plasmid vector (Figure 1I). This effect is not the indirect result of a lower invasion efficiency as the *tepP* mutant did not display a defect in synchronized entry in non-confluent or polarized A2EN cells (Figures 1J and 1K). In contrast, *tmeA* and *tarP* mutants had no impact on cell dispersion. These mutants exhibited defects in host cell entry in non-polarized cells as previously reported[22,35]; although those defects were markedly milder in polarized cells (Figures 1J and 1K).

These observations suggest that TepP functions may be most relevant in polarized epithelial cells. Indeed, inactivation of *tepP* significantly reduced the production of infectious units (IFUs) in A2ENs but not HeLa cells.[26] To assess if TepP was important during animal infections, we challenged mice transcervically with wild-type or *tepP* mutant CTL2, the strain most tractable for genetic manipulation, and measured bacterial burdens over time in the upper genital tract (UGT). The *tepP* mutant was cleared at a faster rate than wild-type bacteria from the genital tract (Figure 1L), indicating that TepP plays an important role in *Chlamydia* survival in host tissues.

TepP promotes the tyrosine phosphorylation of the host actin-binding protein EPS8

TepP alters the global pattern of tyrosine phosphorylated (p-Tyr) proteins during the first 12 h of infection.[20,26] By immunofluorescence microscopy, we observed a significant TepP-dependent spatial redistribution of p-Tyr proteins in *Chlamydia* infected cells (Figure 2A). To identify p-Tyr proteins, A2EN cells were mock-infected or infected with either a *tepP* null mutant complemented with TepP (pTepP) or an empty vector (pVector), subjected to immunoprecipitation with anti-phospho-Tyr antibodies (Figure 2B), and processed for a quantitative proteomic analysis by LC/MS-MS (Figure 2C). A pathway enrichment analysis of the Tyr phosphoproteomes of cells infected with TepP$^+$ or TepP$^-$ *Chlamydia* indicated that components of the Rho/Ras-mediated signaling pathways, regulation of cytoskeletal dynamics, and cell motility were significantly overrepresented among p-Tyr proteins (Figure 2D). Similar results were obtained when comparing mock-infected to cells infected with TepP$^+$ *Chlamydia*, indicating that TepP centrally regulates Tyr-based signaling (Figures S1A and S1B; Table S1). We also identified TepP-independent p-Tyr proteins involved in cytoskeletal organization, namely focal adhesion kinase (FAK1) (Figures S1C and S1D; Table S1), a putative interactor of the effector TarP.[36]

The most prominent targets of TepP-dependent phosphorylation were the host actin-binding protein EPS8 and EPS8 Like 2 (EPS8L2) (Figure 2C; Table S1). EPS8 was first identified as a substrate of EGFR signaling and as a regulator of EGF internalization, Rab5-dependent endocytic trafficking, and Rac1-based signaling.[37,38] The C-terminal domain of EPS8 contains an actin-capping and bundling domain,[39,40] which promotes the assembly of actin-rich structures, such as stereocilia, filopodia, and microvilli.[33,34,41] To confirm if EPS8 is phosphorylated in a TepP-dependent manner, we immunoprecipitated EPS8 from A2EN cells infected with wild-type *Chlamydia*, a *tepP* mutant, or its complemented version, followed by immunoblotting with anti-pTyr antibodies. Phosphorylation of EPS8 was detected in A2EN cells infected with *Chlamydia* expressing TepP but not uninfected cells or cells infected with *tepP* mutants (Figures 2E and 2F). We

Please cite this article in press as: Dolat et al., *Chlamydia* repurposes the actin-binding protein EPS8 to disassemble epithelial tight junctions and promote infection, Cell Host & Microbe (2022), https://doi.org/10.1016/j.chom.2022.10.013

CellPress

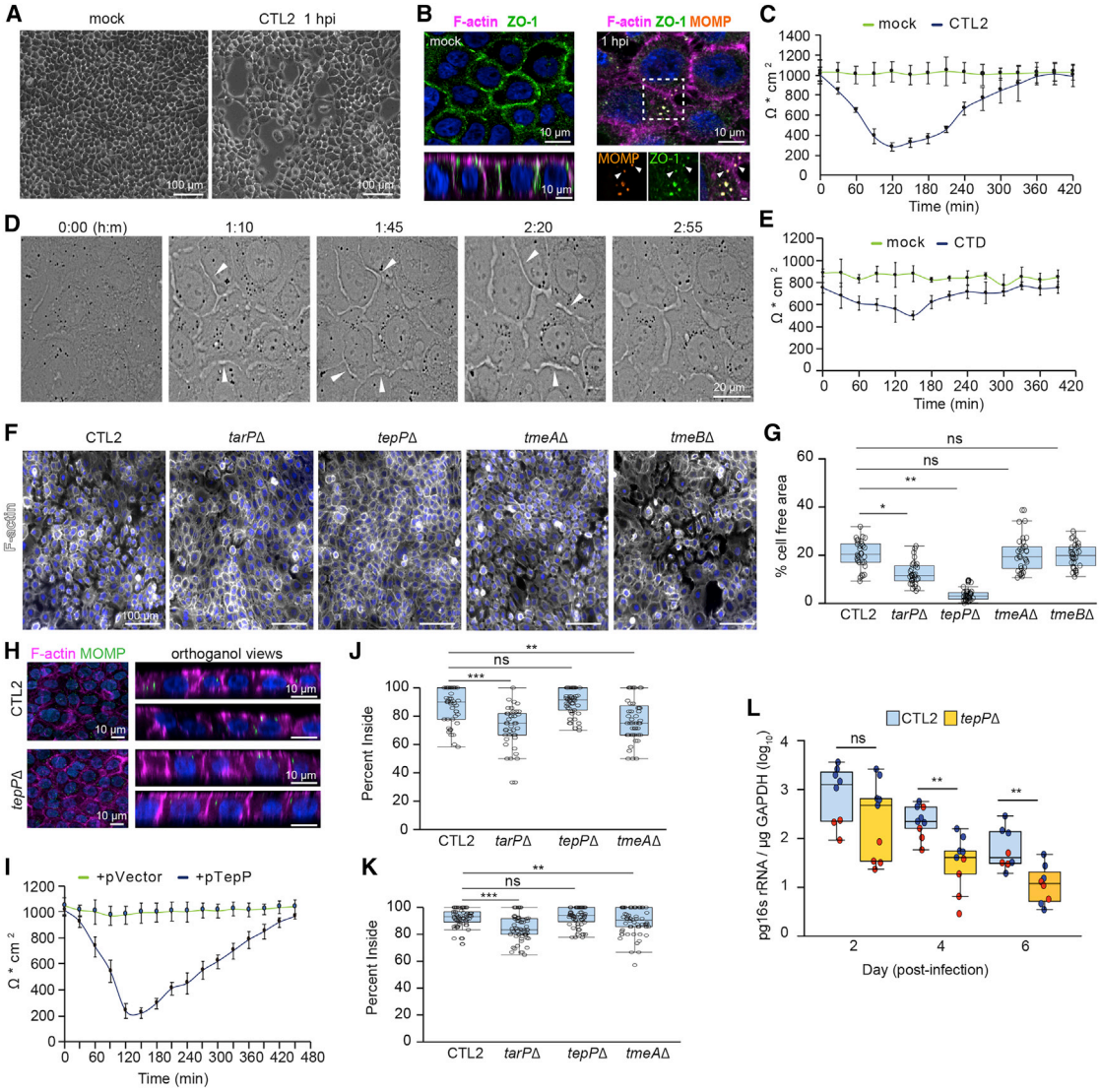

Figure 1. The *Chlamydia* effector TepP modulates epithelial tight junctions and promotes cell dispersion

(A–E) *C. trachomatis* disrupts tight junctions and promotes epithelial cell dispersion. (A) Phase contrast images of polarized A2EN cells on collagen-coated coverslips infected with CTL2 for 1 h. (B) Confocal images of polarized A2EN cells on collagen-coated filters infected with CTL2 for 1 h and stained for ZO-1 (green), F-actin (magenta), *C. trachomatis* major outer membrane protein (MOMP; orange), and DNA (blue). Arrows denote ZO-1-positive inclusions near disassembling tight junctions. Mock represents uninfected cells. Inset scale bar, 1 µm. (C) Transepithelial electrical resistance (TEER) was measured every 30 min for 7 h in polarized A2EN cells infected with CTL2 (n = 3). Data are represented as the mean ± SD. (D) Still frames from time-lapse microscopy of A2EN cells infected with CTL2. Arrows denote gaps forming between cells. Time display, hours:minutes (E) TEER was measured every 30 min for 7 h in polarized A2EN cells mock-infected or infected with *C. trachomatis* serovar D (CTD) (n = 3). Data are represented as the mean ± SD.

(F–I) TepP is required for tight junction disruption and epithelial cell dispersion. (F) Fluorescence images of polarized A2EN cells on collagen-coated coverslips infected with the indicated strain for 1 h and stained for F-actin (white) and DNA (blue). (G) Quantification of the percent of cell-free area (n = 30 fields of view; unpaired, two-tailed t test). (H) Maximum projections and orthogonal views from confocal images of A2EN cells polarized on collagen-coated filters infected with CTL2 or *tepP* mutant bacteria for 1 h and stained for MOMP (green), F-actin (magenta), and DNA (blue). (I) TEER was measured every 30 min for 7 h in polarized A2EN cells infected with a *tepP* mutant or its complemented counterpart (n = 3). Data are represented as the mean ± SD.

(J and K) TepP does not regulate synchronized host cell entry. Non-confluent (J) or polarized (K) A2EN cells were infected with the indicated strain for 30 min and processed for inside-outside staining as a measure of cell invasion. Quantification shows the percent of EBs inside the cell (n = 60 cells; Welch's t test).

(L) TepP-deficient C. trachomatis CTL2 are cleared faster from the mouse genital tract. Quantification of normalized bacterial genome counts at the indicated time (n = 8–9 mice per time point, Mann-Whitney U test). Color indicates values from two independent experiments.

(G, J, and K) Box and Whisker plots represent the median and interquartile range (IQR) ± either 1.5*IQR or min and max values.

*p < 0.05, **p < 0.01, ***p < 0.001, ****p < 0.0001.

Please cite this article in press as: Dolat et al., *Chlamydia* repurposes the actin-binding protein EPS8 to disassemble epithelial tight junctions and promote infection, Cell Host & Microbe (2022), https://doi.org/10.1016/j.chom.2022.10.013

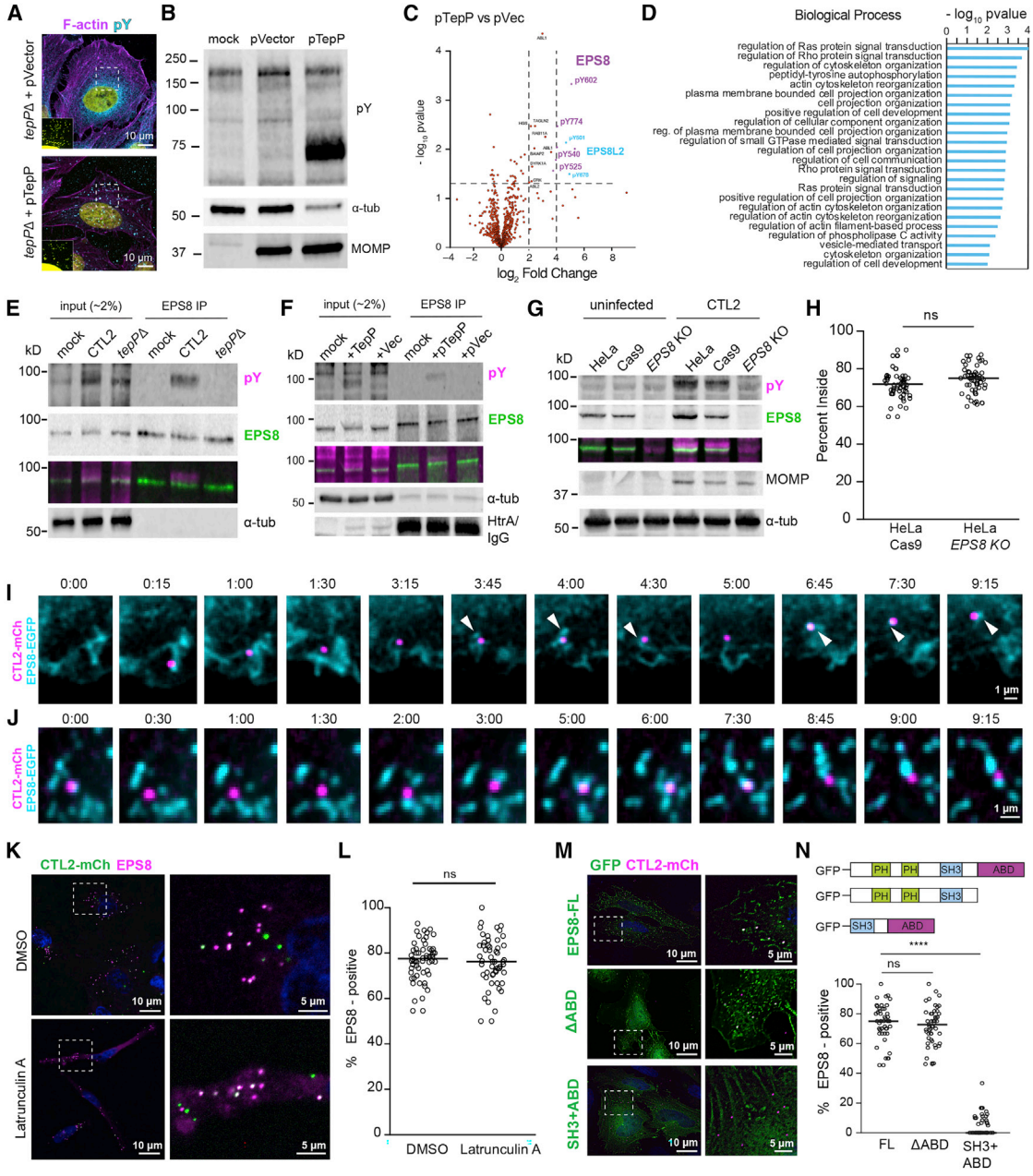

Figure 2. TepP alters the tyrosine phosphorylation profile of host proteins and prominently targets the actin-binding protein EPS8

(A–D) TepP alters the host cell phosphoproteome. (A) Confocal images of HeLa cells infected with the indicated strain for 1 h and stained for pTyr (cyan), F-actin (magenta), and DNA (yellow). Inset shows enhanced DNA signal to show inclusions. (B) Whole cell lysates from A2EN cells infected with *tepP* mutants transformed with pVector or pTepP and subjected to western blot analysis for pTyr, MOMP, and α-tubulin. (C) Volcano plot representing the change in abundance of Tyr phospho-peptides from A2EN cells infected with a *tepP* mutants transformed with pTepP versus pVector. (D) Bar graph depicts a gene ontology enrichment analysis of biological processes for differentially phosphorylated proteins.

(E–G) TepP regulates the Tyr phosphorylation of EPS8. EPS8 was immunoprecipitated from A2EN cells infected with CTL2 or *tepP* mutant bacteria (E) or *tepP* mutants transformed with pTepP or pVec (F) for 1 h and subjected to western blot analysis for pTyr, EPS8, α-tubulin, and *Chlamydia* HtrA. (G) Whole cell lysates HeLa, HeLa^{Cas9}, and HeLa^{Cas9} *EPS8* KO cells uninfected or infected for 2 h were subjected to western blot analysis for pTyr, EPS8, MOMP, and α-tubulin.

(H) EPS8 is not required for synchronized entry into host cells. Quantification of the percent CTL2 EBs inside in HeLa^{Cas9} and HeLa^{Cas9} *EPS8* KO cells at 30 min post-infection (n = 57–58 cells; unpaired, two-tailed t test).

(I and J) EPS8 localizes at sites of CTL2 invasion and early inclusion trafficking. Time-lapse still frames from MEF (I) and HeLa cells (J) expressing GFP-EPS8 (cyan) infected with CTL2-mCh (magenta) and imaged by spinning disk microscopy. Time display, min:sec.

(K–N) EPS8 recruitment to early inclusions is actin-independent. (K) Fluorescence images of HeLa cells infected with CTL2-mCh (green), incubated with DMSO or Latrunculin A for 1 h, and stained for EPS8 (magenta) and DNA (blue). (L) Quantification of EPS8-positive inclusions (n = 54–56 cells; unpaired, two-tailed t test).

(legend continued on next page)

Please cite this article in press as: Dolat et al., *Chlamydia* repurposes the actin-binding protein EPS8 to disassemble epithelial tight junctions and promote infection, Cell Host & Microbe (2022), https://doi.org/10.1016/j.chom.2022.10.013

further confirmed EPS8 as a major target of TepP-dependent Tyr phosphorylation by infecting HeLa cells where *EPS8* had been inactivated by CRISPR-Cas9-mediated gene editing (Figure 2G). Although EPS8 was previously reported to localize to sites of *C. trachomatis* invasion and siRNA-mediated silencing of EPS8 expression reduced entry,[25] we found no significant difference in invasion efficiencies between HeLa^{Cas9} and HeLa^{Cas9} *EPS8* KO cells (Figure 2H). Using time-lapse imaging, we monitored EGFP-EPS8 localization during the initial stage of *C. trachomatis* invasion and found that EPS8 is transiently recruited to *Chlamydia* EBs during entry and dissociates quickly before a more stable pool of EPS8 associates with nascent inclusions (Figure 2I; Video S2). This stable pool exhibits dynamic behavior where tubular-like EPS8 elements emanate from and associate with early inclusions (Figure 2J; Video S3).

TepP regulates the recruitment of EPS8 to early inclusions in an actin- and phosphorylation-independent manner

Because *C. trachomatis* stimulates actin polymerization during invasion, we first assessed if EPS8 recruitment to inclusion was an indirect consequence of its binding to actin filaments. We observed no difference in EPS8 recruitment to early inclusions in cells treated Latrunculin A, which disassembles actin filaments (Figures 2K and 2L). We next generated EGFP-tagged EPS8 constructs lacking various functional domains and tested their ability to localize to the nascent inclusion. The actin-binding domain (ABD) was dispensable for the recruitment of EPS8 to nascent inclusions (Figures 2M and 2N). Similarly, the EPS8 C-terminal SH3 and ABD alone did not localize to inclusions (Figures 2M and 2N), although the SH3 domain interacts with Abi1, which localizes to *Chlamydia* entry sites.[25] Altogether, these observations imply that EPS8 recruitment to early inclusions is uncoupled from its F-actin-binding properties.

Given the role of TepP in regulating EPS8 modifications, we posited that the recruitment of EPS8 to inclusions would be dependent in TepP. Indeed, TepP and EPS8 colocalized in punctate and tubule-like structures at the nascent inclusion (Figure 3A). EPS8 localization to the inclusion occurred only early in infection, rapidly diminished by 12 h and was absent from inclusions by 20 h (Figures 3B and 3C), which correlates with the kinetics of TepP secretion and phosphorylation.[20] We next infected A2EN cells with *C. trachomatis* mutants lacking effectors that are translocated early in infection. We found that a strain lacking TepP abolished EPS8 recruitment while *tarP* and *tmeA* mutants showing only slight reductions in their association with EPS8 (Figures 3D and 3E) (Figure 1). Moreover, we determined that the recruitment of EPS8 to nascent inclusions is spatially restricted by TepP. Co-infections with *tepP* mutant and wild-type bacteria indicated that within a single epithelial cell EPS8 was only recruited to wild-type bacteria (Figures 3F and 3G).

We next expressed TepP in HeLa cells and found that EPS8 relocalized to TepP-positive tubulovesicular structures (Figure 3H). The colocalization of TepP and EPS8 in transfected cells was independent of F-actin, as it was resistant to actin depolymerization with Latrunculin A (Figure S2A) and did not require the ABD of EPS8 (Figure S2B). Furthermore, TepP and EPS8 co-expressed in 293T cells co-immunoprecipitated, suggesting an association between TepP and EPS8 (Figure 3G). Despite TepP driving the Src-dependent phosphorylation of EPS8,[26,42] we did not observe differences in the recruitment of EPS8 to nascent inclusions in fibroblasts deficient in Src-family kinases (Src/Fyn/Yes) (Figures S2C and S2D). Furthermore, we mutated the four Tyr residues to Phe in EGFP-EPS8 and determined that this variant still co-immunoprecipitated with TepP with similar efficiency as wild-type EPS8 (Figure 3I), co-localized to nascent inclusions (Figures S2E and S2F), and associated with ectopically expressed TepP (Figure S2G). Taken together, these data indicate that TepP associates with EPS8 in an actin- and phospho-Tyr-independent manner.

TepP and EPS8 are required for *Chlamydia*-mediated modulation of epithelial morphology and the disruption of tight junctions and barrier function

Although the association between TepP and EPS8 did not require F-actin polymerization, we postulated that this interaction could influence cytoskeletal dynamics, given the role of EPS8 in F-actin bundling and capping. Indeed, we observed that *Chlamydia* infection impacted epithelial cell morphology and that HeLa cells infected with wild-type *Chlamydia*, but not *tepP* mutants, became elongated with an increased aspect ratio early in infection (Figures 4A and 4B). TepP was sufficient to stimulate these morphological alterations as ectopic expression of TepP in HeLa cells increased the cell aspect ratio (Figures 4C and 4D). To test if TepP drives these changes in cell shape through EPS8, we transfected HeLa^{Cas9} and HeLa *EPS8* KO cells with vectors expressing mCh or TepP-mCh. EPS8-deficient HeLa cells exhibited elongated cell shape compared with the parental HeLa^{Cas9} cells (Figures 4E–4G), but the expression of TepP did not significantly change the cell aspect ratio between the HeLa^{Cas9} and HeLa *EPS8* KO cells (Figures 4F and 4G). Taken together, these data show that TepP acts through EPS8 to modify epithelial cell shape.

To determine if the interaction between TepP and EPS8 is important for the epithelial dispersion phenotype observed in polarized A2EN cells, we generated Cas9-expressing A2EN cells (A2EN^{Cas9}) and deleted EPS8 by CRISPR-Cas9 editing (Figures 4H and 4I). Depletion of *EPS8* did not affect the formation of tight and adherens junctions or the establishment of epithelial barrier functions as assessed by TEER over 10 days (Figures 4I, 4J, S3A, and S3B). However, A2EN *EPS8* KO cells were resistant to tight junction disruption during early infection (Figures 4K–4M), although they were as permissible for *Chlamydia* invasion as the A2EN^{Cas9} parental cells (Figure 4N). In endometrial organoids, a model that more closely recapitulates the polarized epithelia of the UGT, nascent inclusions disrupt adherens junctions and recruits the tight junction scaffolding protein ZO-1,[7] which may underlie the disruption of tight junctions.

(M) Fluorescence images of HeLa cells expressing GFP-tagged EPS8 (green) or indicated deletions were infected with CTL2-mCh (magenta) for 1 h and stained for DNA (blue). (N) Quantification of EPS8-positive inclusions (n = 47–63 cells; unpaired, two-tailed t test).
(H, L, and N) Scatter plots represent individual cells, and the line denotes the median.
****$p < 0.0001$.

Please cite this article in press as: Dolat et al., *Chlamydia* repurposes the actin-binding protein EPS8 to disassemble epithelial tight junctions and promote infection, Cell Host & Microbe (2022), https://doi.org/10.1016/j.chom.2022.10.013

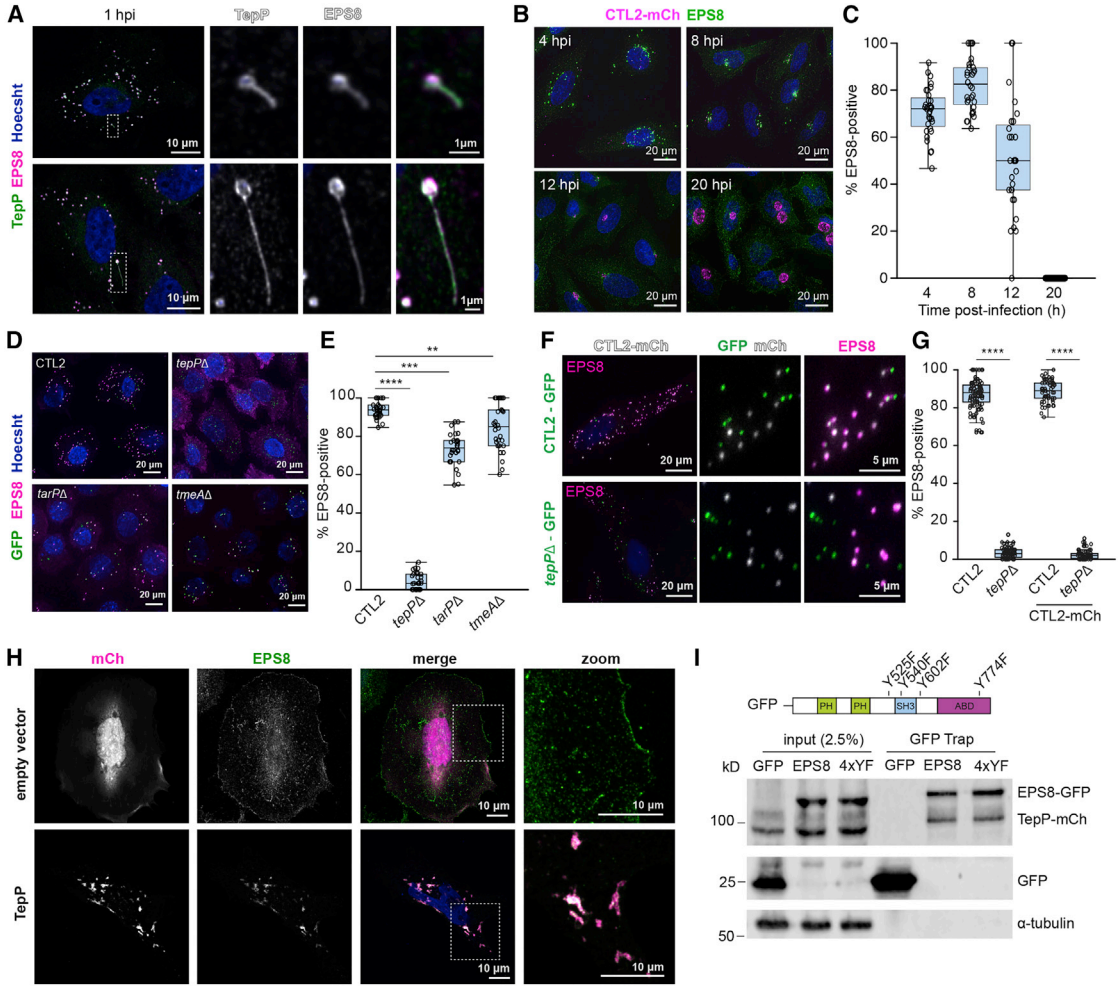

Figure 3. TepP associates with EPS8 on early inclusions

(A–C) Morphology and association of EPS8 with inclusions. (A) Confocal images of HeLa cells infected with CTL2 for 1 h and stained for TepP (green), EPS8 (magenta), and DNA (blue). (B) Fluorescence images of HeLa cells infected with CTL2-mCh (magenta) for the indicated time and stained for EPS8 (green) and DNA (blue) and (C) quantification of EPS8-positive inclusions over time (n = 32 cells).

(D–G) TepP is required for EPS8 recruitment to early inclusions. (D) Fluorescence images of A2EN cells infected with the indicated GFP-expressing strain (green) and stained for EPS8 (magenta) and DNA (blue). (E) Quantification of EPS8-positive inclusions (n = 30 cells; unpaired, two-tailed t test). (F) Fluorescence images of HeLa cells co-infected with GFP-expressing CTL2 (top) or *tepP* mutant (bottom) bacteria (green) and CTL2-mCh (white) for 1 h and immunostained for EPS8 (magenta) and DNA (blue). (G) Quantification of EPS8-positive inclusions within co-infected cells (one strain, n = 69 cells; two strains, n = 55–57 cells; unpaired, two-tailed t test).

(H and I) Ectopic expression of TepP drives the relocalization of EPS8. (H) Confocal images of HeLa cells transfected with mCh or mCh-TepP and stained for EPS8 (green) and DNA (blue). (I) Co-immunoprecipitation of EPS8 and TepP. Whole cells lysates of 293T cells co-expressing mCh-TepP with EGFP or EGFP-EPS8 were immunoprecipitated using the GFP Trap system and subjected to western blot analysis for GFP, mCh, and α-tubulin.

(C, E, and G) Box and Whisker plots represent the median and interquartile range ± either the min and max values or 1.5*IQR.

**p < 0.01, ***p < 0.001, ****p < 0.0001.

Indeed, ZO-1 was recruited robustly to nascent inclusions in polarized A2EN^{Cas9} cells but not A2EN *EPS8* KO cells (Figures 4O and 4P). Reciprocally, we found that TepP is required for the recruitment of ZO-1 (Figures 4Q and 4R). The disruption to epithelial organization was not limited to tight junctions as TepP and EPS8 were also required for the disassembly of adherens junctions (Figures S3C and S3D). Tight junctions were eventually repaired as ZO-1 localization to the inclusion diminished over time and correlated with the recovery of TEER (Figures S3E and S3F).

We next assessed the impact of EPS8 in TepP-mediated disruption of tight junction in the endometrial organoid infection model. In endometrial organoids, TepP was essential for remodeling epithelial organization and reducing epithelial barrier function, as assessed by the leakage of fluorescent dextran from the lumen of infected organoids (Figures 5A–5D; Video S4). EPS8 localized to the apical domain of polarized endometrial epithelia (Figure 5E), where it is known to regulate microvilli elongation. As in A2EN cells, TepP was required for the recruitment of EPS8 to nascent inclusions in endometrial organoids (Figures 5F and 5G).

Please cite this article in press as: Dolat et al., *Chlamydia* repurposes the actin-binding protein EPS8 to disassemble epithelial tight junctions and promote infection, Cell Host & Microbe (2022), https://doi.org/10.1016/j.chom.2022.10.013

CellPress

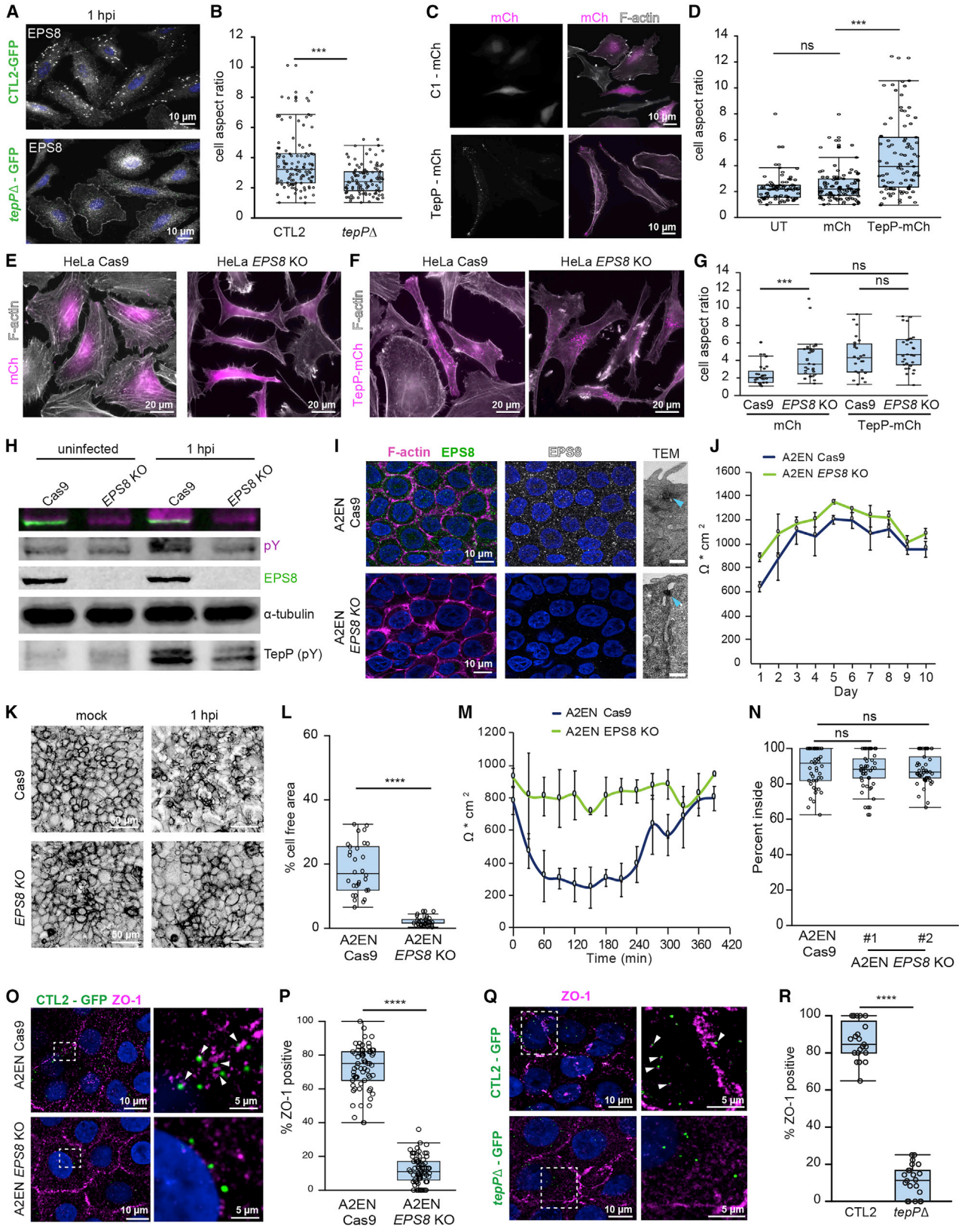

(legend on next page)

Please cite this article in press as: Dolat et al., *Chlamydia* repurposes the actin-binding protein EPS8 to disassemble epithelial tight junctions and promote infection, Cell Host & Microbe (2022), https://doi.org/10.1016/j.chom.2022.10.013

We next disrupted the *Eps8* exon 4 in mice by CRISPR-Cas9-mediated gene editing (Figure 5H) and derived organoids from $Eps8^{+/+}$ and $Eps8^{-/-}$ mice. These organoids were morphologically indistinguishable (Figures S4B–S4F). Infections of $Eps8^{+/+}$ organoids, but not $Eps8^{-/-}$, with *C. trachomatis* led to the disruption of epithelial organization (Figure 5I). Epithelial cell disruption is likely conserved among TepP-expressing *Chlamydia* species as organoids infected with *Chlamydia muridarum*, a mouse adapted pathogen, also significantly impacted epithelial organization (Figure 5J) in $Eps8^{+/+}$ but not $Eps8^{-/-}$ organoids. Moreover, tight junctions were preserved in $Eps8^{-/-}$ organoids during early infection and maintain their barrier functions in dextran leakage assays (Figures 5K–5M; Video S5). These findings are consistent with a model, wherein TepP requires EPS8 to disrupt cell-cell junctions during invasion in cell culture and organoid models.

The disruption of tight junctions promotes *Chlamydia* entry into polarized epithelia

Time-lapse microscopy of polarized A2EN cells labeled with fluorescent SiR-actin and infected with GFP-expressing *C. trachomatis* indicated that EBs often land and enter near sites of junction remodeling (Figure 6A; Video S5). We hypothesized that the disruption of tight junctions can promote entry of *Chlamydia* at newly exposed basolateral receptors. Therefore, we developed an assay to assess the impact of an initial infection on subsequent ones (Figure 6B). Polarized A2EN cells were first infected synchronously with a GFP-expressing wild-type or *tepP* mutant *Chlamydia* for 1.5 h followed by an asynchronous infection with non-fusogenic mCh-expressing *Chlamydia incA* mutants. Because the non-fusogenic *incA* mutant makes independent inclusions, the efficiency of secondary invasions can be determined by quantifying the number of mCh-positive inclusions. We observed that epithelial cell dispersion during a primary infection with wild-type *Chlamydia* enhanced the number of secondary inclusions compared with primary infections with *tepP* mutants (Figure 6C). Similarly, polarized A2EN *EPS8* KO cells were less permissive for secondary invasion events compared with the parental $A2EN^{Cas9}$ controls (Figure 6D). Importantly, primary infections with *Chlamydia tepP* mutants showed no further decrease in the number of secondary inclusions formed in A2EN *EPS8* KO cells (Figure 6E), providing additional support to the premise that monolayer remodeling by TepP occurs largely through EPS8. Finally, the primary infection did not affect the number of secondary inclusions formed when infections were performed in non-polarized A2EN cells (Figure 6F), further indicating that this effect is unique to polarized cells.

To test whether TepP was sufficient to promote entry through the disruption of cell junctions, we used Madin-Darby Canine Kidney (MDCK-I) cells, an epithelial model that is recalcitrant to *Chlamydia* infection when polarized (Figure 6G).[43] First, we determined that TepP expression in MDCK-1 cells increased EPS8 localization to the lateral membrane and disrupted ZO-1 positive tight junctions (Figure S5A–S5D). Moreover, TepP-positive punctate and tubulovesicular structures co-localized with EPS8 at tight junctions and in areas of junction remodeling (Figure S5E). Consistent with these observations, TepP expression delayed monolayer formation and reduced TEER during MDCK polarization (Figures S5F and S5G). In this model, TepP expression in polarizing MDCK cells significantly enhanced *Chlamydia* infection (Figure 6H). Importantly, wild-type and *tepP* mutant *Chlamydia* invaded TepP-expressing MDCK cells with equivalent efficiency (Figure 6I) and inclusions were preferentially found in cells expressing TepP-mCh (Figures 6J and 6K).

TepP and EPS8 promotes *Chlamydia* shedding and survival in the murine genital tract

Our results indicate that TepP and EPS8 regulate epithelial organization during *C. trachomatis* entry and that TepP prolonged the survival of CTL2 strains following a transcervical challenge. In A2EN *EPS8* KO cells, *C. trachomatis* inclusions were significantly smaller than in the parental lines, and there was a marked reduction in the production of IFUs (Figures 7A–7C). However, IFU production of CTL2 *tepP* mutants in A2EN *EPS8* KO cells was still lower than wild-type CTL2, indicating that TepP targets other host processes that are important for IFU production

Figure 4. TepP and EPS8 modulate cell morphology and promote the disruption of tight junctions

(A and B) TepP promotes epithelial cell elongation during infection. (A) Fluorescence images of HeLa cells infected with GFP-expressing CTL2 or *tepP* mutant bacteria (green) for 1 h and stained for EPS8 (white). (B) Quantification of the cell aspect ratio (n = 106–110 cells; unpaired, two-tailed t test).

(C–G) TepP-dependent elongation of epithelial cell requires EPS8. (C) Fluorescence images of HeLa cells expressing mCh or mCh-TepP (magenta) and stained for F-actin (white). (D) Quantification of the cell aspect ratio (n = 106–112 cells; unpaired, two-tailed t test). (E and F) Fluorescence images of $HeLa^{Cas9}$ or $HeLa^{Cas9}$ *EPS8* KO cells expressing mCh or mCh-TepP and stained for F-actin (white). (G) Quantification of the cell aspect ratio (n = 24–32 cells; unpaired, two-tailed t test).

(H–M) EPS8 is required for the dispersion of polarized A2EN cells. (H) Whole cell lysates from uninfected and infected $A2EN^{Cas9}$ and $A2EN^{Cas9}$ *EPS8* KO cells were subjected to western blot analysis for EPS8, pTyr, and α-tubulin. (I) Confocal images of $A2EN^{Cas9}$ and $A2EN^{Cas9}$ *EPS8* KO cells immunostained for EPS8 (green), F-actin (magenta), and DNA (blue). Transmission electron micrographs of the lateral membrane contacts showing apical tight junctions (blue arrows). Scale bars, 0.5 μm. (J) TEER measurements in $A2EN^{Cas9}$ and $A2EN^{Cas9}$ *EPS8* KO cells over 10 days. Data are represented as the mean ± SD (n = 3). (K) Confocal images of polarized $A2EN^{Cas9}$ or $A2EN^{Cas9}$ *EPS8* KO cells mock-infected or infected with CTL2 for 1 h and stained for F-actin and quantification of cell-free area (L) (n = 30 fields of view; unpaired, two-tailed t test). (M) TEER was measured every 30 min for 7 h in polarized $A2EN^{Cas9}$ and $A2EN^{Cas9}$ *EPS8* KO cells infected with CTL2. Data are represented as the mean ± SD (n = 3).

(N) EPS8 is not required for synchronized entry into A2EN cells. $A2EN^{Cas9}$ or $A2EN^{Cas9}$ *EPS8* KO cells were infected with CTL2 for 30 min and processed for inside-outside staining. Quantification of the percent of EBs inside (n = 30 cells; unpaired, two-tailed t test).

(O–R) EPS8 and TepP are required for the recruitment of ZO-1 to early inclusions. (O) Confocal images of $A2EN^{Cas9}$ and $A2EN^{Cas9}$ *EPS8* KO cells infected with CTL2-GFP (green) and stained for ZO-1 (magenta) and DNA (blue) and quantification of the percent of ZO-1 positive inclusions (n = 66–74 cells, unpaired, two-tailed t test) (P). (Q) Confocal images of $A2EN^{Cas9}$ infected with GFP-expressing CTL2 or *tepP* mutant bacteria (green) and stained for ZO-1 (magenta) and DNA (blue) and quantification of the percent ZO-1-positive inclusions (n = 22–23 cells; unpaired, two-tailed t test) (R). Arrows denote ZO-1 localization to nascent inclusions.

Box and Whisker plots represent the median and interquartile range ± min and max values (L and P) or 1.5*IQR (B, D, G, N, and R).

***p < 0.001, ****p < 0.0001.

Please cite this article in press as: Dolat et al., *Chlamydia* repurposes the actin-binding protein EPS8 to disassemble epithelial tight junctions and promote infection, Cell Host & Microbe (2022), https://doi.org/10.1016/j.chom.2022.10.013

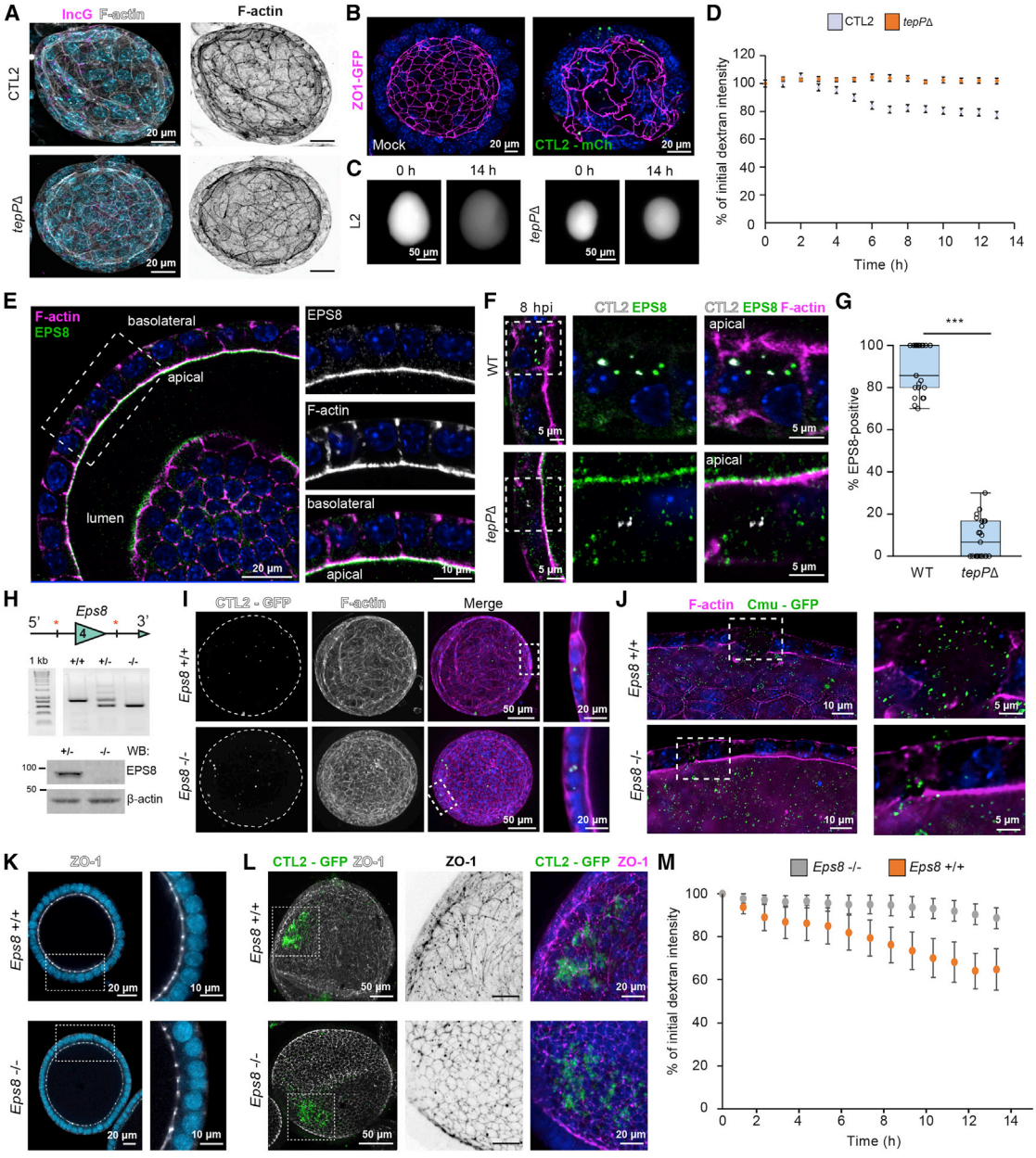

Figure 5. TepP promotes EPS8-dependent epithelial barrier disruption in endometrial organoids

(A–D) TepP is required for organoid barrier disruption. (A) 3D reconstruction of confocal images of endometrial organoids infected with CTL2 or *tepP* mutant bacteria for 8 h and stained for *Chlamydia* IncG (magenta), F-actin (white), and DNA (blue). (B) Confocal images of ZO1-GFP (magenta) organoids uninfected or infected with CTL2-mCh (green) for 14 h and stained for DNA (blue). (C) Endometrial organoids were injected with CTL2 or *tepP* mutant bacteria diluted in fluorescent dextran (white) and imaged live for 14 h. Still frames from the start and end of imaging are shown. (D) Quantification of luminal dextran intensity over time (n = 11 organoids).

(E–G) TepP is required for EPS8 recruitment to early inclusions in endometrial organoids. (E) Confocal image from a medial section of an endometrial organoid stained for EPS8 (green), F-actin (magenta), and DNA (blue). (F) Confocal images of organoids infected with CTL2 or *tepP* mutant bacteria (white) for 8 h and stained for EPS8 (green), F-actin (magenta), and DNA (blue). (G) Quantification of EPS8-positive inclusions (n = 23 cells; unpaired, two-tailed t test). Box and Whisker plots represent the median and interquartile range ± min and max values.

(H–M) EPS8 is required for infection-mediated disruption of epithelial barrier in organoids. (H) Top: schematic of exon targeting of the mouse *Eps8* locus. Middle: PCR analysis of exon 4 deletion in wild-type, heterozygous, and knockout mice. Bottom: western blot analysis of primary endometrial fibroblasts from heterozygous or knockout mice with anti-EPS8 and β-actin antibodies. (I) Confocal images of $Eps8^{+/+}$ or $Eps8^{-/-}$ organoids infected with GFP-expressing CTL2 (green) for 4 h and stained for F-actin (magenta) and DNA (blue). (J) Fluorescence images of $Eps8^{+/+}$ or $Eps8^{-/-}$ organoids infected with GFP-expressing *C. muridarum* (green) for 4 h and stained for F-actin (magenta) and DNA (blue). (K and L) Confocal images of $Eps8^{+/+}$ or $Eps8^{-/-}$ organoids uninfected (K) or

(legend continued on next page)

Please cite this article in press as: Dolat et al., *Chlamydia* repurposes the actin-binding protein EPS8 to disassemble epithelial tight junctions and promote infection, Cell Host & Microbe (2022), https://doi.org/10.1016/j.chom.2022.10.013

(Figure 7D). Because of the limitations of mouse models for human *Chlamydia* UGT infections,[44] we tested the role of EPS8 in *Chlamydia* survival and pathogenesis for the highly related mouse pathogen *C. muridarum*. *Eps8*$^{+/+}$ and *Eps8*$^{-/-}$ littermates were infected intravaginally with *C. muridarum* and bacterial shedding was assessed every 3–4 days. The number of recoverable IFUs from vaginal swabs was consistently higher in wild-type mice and persisted longer (Figure 7E), further supporting a pro-infection role for EPS8.

We next generated a *tepP* mutant in *C. muridarum* (Figure S6A), which phenocopies *C. trachomatis tepP* mutants in that it failed to recruit EPS8 to early inclusions and promote dispersion of polarized A2EN cells (Figures S6B–S6D). *C. muridarum tepP* mutants were also significantly impaired in the production of IFUs in mouse fibroblast cells (Figure 7G) and did not ascend to the UGT after vaginal infections with complete clearance within 6 days (Figure 7H). We next bypassed the lower genital tract by infecting mice transcervically and found *tepP* mutant EBs were shed for up to 12 days, albeit at significantly lower levels than wild-type *C. muridarum* (Figure 7I). Moreover, the uterine horns and ovaries exhibited significantly reduced acute pathology (Figures 7K and 7L). To test whether the decrease in bacterial burden in the UGT for *C. muridarum tepP* mutants was dependent on EPS8-mediated manipulation of host functions, we compared bacterial shedding between infected *Eps8*$^{+/+}$ and *Eps8*$^{-/-}$ littermates. The level of bacterial shedding was lower in Eps8 KO mice and the infection was cleared faster (Figure 7M). Furthermore, IFU production of the *tepP* mutant was again significantly reduced in the absence of EPS8 (Figure 7N). Collectively, these data indicate that EPS8 promotes infection and that TepP performs additional functions that are also important for successful colonization of the UGT.

DISCUSSION

C. trachomatis disrupts epithelial cell organization and cell-cell junctions in cell culture,[7,8,45] but the mechanisms underlying this process or consequences to infection are largely unknown. Here, we report that the effector TepP transiently disrupts epithelial tight junction organization to promote host cell entry. We propose based on live imaging (Figure 6A) and secondary infection assays (Figure 6B) that TepP-mediated disruption of cell junctions and polarity increases the availability of basolateral receptors that enhance the binding and entry of additional bacteria. A similar process has been documented during *Pseudomonas aeruginosa* infection in polarized MDCK cells, where the bacterium alters epithelial polarity by stimulating the positioning of basolateral components to the apical surface to promote colonization.[46] Similarly, the Coxsackie virus activates Src and Abl kinases and Rho GTPase signaling to reorganize the actin cytoskeleton and bind to the Coxsackie and Adenovirus receptor (CAR), a tight junction component that is necessary for virus entry in intestinal epithelial cells.[47] *C. trachomatis* binds to heparan sulfate proteoglycans that are largely localized to the basolateral compartment of polarized epithelia in the female reproductive tract,[48–50] supporting the notion that altering epithelial polarity can increase EB binding, but further studies are necessary to identify the mechanism of host receptor reorganization.

Chlamydia infection modulates Tyr phosphorylation-mediated signaling.[51,52] In addition, TarP and TepP themselves are major effector proteins that are also targets of Tyr phosphorylation by Src kinases.[20,26,53] We compared the impact of *Chlamydia* infection, and TepP, in particular, on the global Tyr phosphoproteome in A2EN epithelial cells. Infection with wild-type *Chlamydia* or *tepP* mutants resulted in higher level of Tyr phosphorylation of receptor tyrosine kinase signaling pathways (e.g., EGFR), regulators of the actin cytoskeleton, and proteins involved in cell motility and morphology as compared with uninfected cells, but the targets did not significantly overlap. For instance, EPS8 and the related EPS8L2, host actin-binding proteins that regulate actin-based structures,[54] emerged as major targets of TepP-dependent phosphorylation (Figure 2C). We determined that EPS8 is recruited to bacterial entry sites and remained strongly associated with nascent inclusions in a manner that is strictly dependent on TepP (Figures 2 and 3). Although EPS8 phosphorylation was not required for its recruitment to nascent inclusion, these phosphorylation sites are in residues that mediate interactions with different host partners involved in cell signaling, endocytosis, vesicle trafficking, cytoskeleton organization,[55] and promote tumor cell growth.[56] It is also possible that TepP-dependent phosphorylation may stabilize EPS8, given its abundance is linked to Src-dependent phosphorylation (Figure S2) as previously reported,[42] and EPS8 levels were reduced during infection in the presence of Src inhibitors (Figure S3F).

TepP expression was sufficient to redistribute EPS8 to internal puncta and induce a change in cellular morphology in HeLa cells (Figures 3 and S2) which parallels what is seen in cells infected with TepP-expressing *Chlamydia* (Figure 1). In transfected MDCK cells, TepP re-localized EPS8 to ZO-1 positive tight junctions and disrupted barrier function (Figure S5). EPS8 is not a canonical regulator of epithelial cell junctions and *Eps8*$^{-/-}$ mice do not exhibit any major phenotypes except for deafness due to defects in auditory cilia.[34] However, EPS8 can interact with tight junction proteins, such as Claudin-4, based on proximity-labeling proteomic approaches.[57] In murine endothelial cells, EPS8 is transiently recruited to adherens junctions upon stimulation to promote VE-cadherin ubiquitination, internalization, and turnover.[58] This latter finding suggests a potential role for EPS8 in the regulated disassembly of junctional complexes. *Chlamydia* appears to have co-opted a similar process to disassemble epithelial cell junctions since ESP8-deficient A2EN cells, which exhibit normal polarization and maintain barrier functions (Figure 4), and endometrial organoids derived from *Eps8*$^{-/-}$ mice were resistant to TepP-mediated disruption of tight junctions.

Our initial observation that *C. trachomatis* CTL2 *tepP* mutants are cleared faster in the murine UGT (Figure 1) gave us impetus to pursue a molecular characterization of TepP. Because this mouse model of human *Chlamydia* infections exhibits a short

infected with CTL2-GFP for 4 h (L) and immunostained for ZO-1 (white) and DNA (blue). (M) Quantification of luminal dextran intensity over time in *Eps8*$^{+/+}$ or *Eps8*$^{-/-}$ organoids infected with CTL2 (n = 9–10 organoids).
(D and M) Data are represented as the mean ± SD.
***$p < 0.001$.

Please cite this article in press as: Dolat et al., *Chlamydia* repurposes the actin-binding protein EPS8 to disassemble epithelial tight junctions and promote infection, Cell Host & Microbe (2022), https://doi.org/10.1016/j.chom.2022.10.013

CellPress

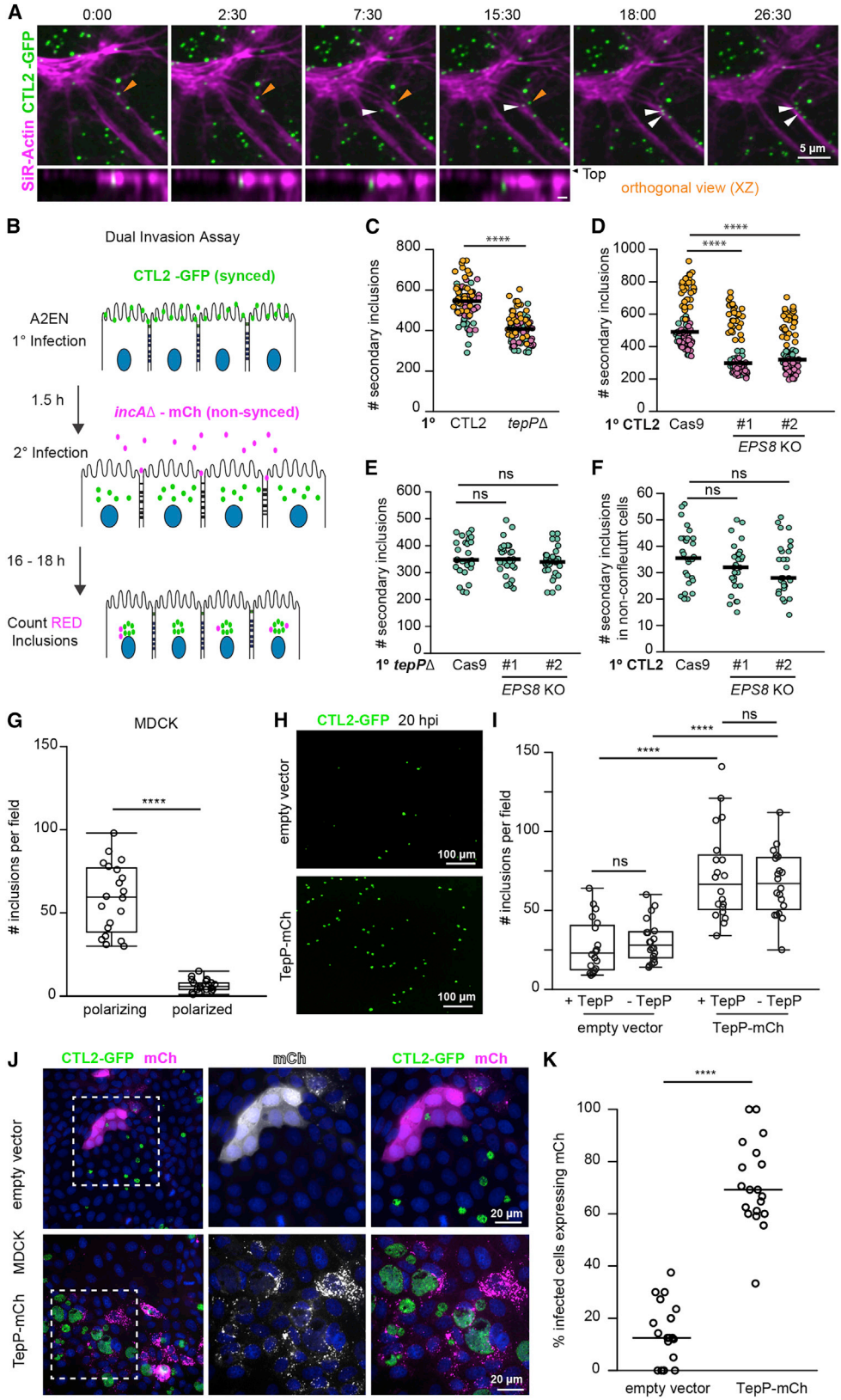

(legend on next page)

kinetic window of bacterial residence in the UGT, we opted to use *C. muridarum*, a mouse adapted *Chlamydia* that infects the vaginal vault and ascends to the UGT where it stimulates pathologies similar to that observed during human infections.[59] *Eps8*$^{-/-}$ mice exhibited lower levels of infection and faster clearance (Figure 6), indicating that EPS8 promotes infection and survival in the UGT. The phenotype of *C. muridarum tepP* mutants, however, was more severe with these mutants being unable to ascend to the UGT after vaginal inoculation and displaying rapid clearance and low pathology if directly inoculated in the UGT. These results suggests that in addition to the manipulation of EPS8, other TepP functions are important for colonization of the reproductive tract. TepP activates Type I interferon responses,[20] which promotes *C. muridarum* infection and pathology in mice,[60] and functions to limit neutrophil recruitment in an endometrial co-culture model with neutrophils.[7] In addition, TepP binds to PI3K and modules the levels of phosphoinositides in infected cells.[26] We postulate that a combination of these additional activities together with the manipulation of tight junctions contribute to the severe virulence defects of *tepP* mutants.

STAR★METHODS

Detailed methods are provided in the online version of this paper and include the following:

- KEY RESOURCES TABLE
- RESOURCE AVAILABILITY
  - Lead Contact
  - Materials availability
  - Data and code availability
- EXPERIMENTAL MODEL AND SUBJECT DETAILS
  - Cell lines and conditioned medium
  - *Chlamydia* strains and propagation
  - Murine infection models
  - Organoid and stromal cell isolation from the mouse endometrium
  - Generation of *Eps8* knockout mice
- METHOD DETAILS
  - Insertional mutagenesis of CTL0063 (*tmeA*), CTL0064 (*tmeB*), and *C. muridarum* TC0268 (*tepP*)
  - *Chlamydia* transformations with shuttle plasmid vectors
  - *Chlamydia* infections in HeLa cells and fibroblasts
  - A2EN polarization, infections, transepithelial electrical resistance (TEER), and live-cell imaging of cell dispersion
  - Endometrial organoid infections
  - MDCK infections, transfections, and TEER
  - CRISPR design, targeting and generation of knockout cell lines
  - Plasmids, primers, mutagenesis, and transfections
  - Time-lapse spinning disk microscopy
  - Determination of infectious progeny
  - Phosphotyrosine profiling in *Chlamydia*-infected A2EN cells
  - Immunoprecipitations
  - Western blots
  - Antibodies
  - Immunofluorescence microscopy and inside-outside staining
  - Transmission electron microscopy
  - Image analysis
  - Quantification of bacterial burden in mice
  - Histological analysis of the female reproductive tract
  - RT-qPCR
- QUANTIFICATION AND STATISTICAL ANALYSIS

SUPPLEMENTAL INFORMATION

Supplemental information can be found online at https://doi.org/10.1016/j.chom.2022.10.013.

ACKNOWLEDGMENTS

We thank Dr. Kenneth Fields (University of Kentucky), Dr. Isabelle Derre (University of Virginia), and Dr. Catherine O'Connell (UNC-Chapel Hill) for *Chlamydia* strains and plasmids; Dr. Matthew Tyska (Vanderbilt University) for plasmids; Dr. Lisa Cameron at the Duke Light Microscopy Core Facility for

Figure 6. The disruption of tight junctions by *Chlamydia* promotes secondary invasion events

(A) Cell invasion at disrupted epithelial cell-cell junctions. Time-lapse still frames of polarized A2EN cells labeled with SiR-actin (magenta) and infected with GFP-expressing CTL2 (green). Time display, min:sec. Arrows denote EBs landing near remodeling cell-cell junctions and moving into cells (orthogonal view).

(B–F) Quantitative assessment of secondary Chlamydia infections upon tight junction disruption. (B) Schematic of experimental workflow to assess secondary infections. Polarized A2EN cells are infected synchronously with GFP-expressing *Chlamydia* (primary infection) before mCh-expressing non-fusogenic *incA* mutant bacteria (secondary infection) was added to the media for an additional 16–18 h. (C) Super plots of the number of secondary inclusions in A2EN cells after primary infection with GFP-expressing CTL2 or *tepP* mutants (n = 90 fields of view, unpaired, two-tailed t tests). (D) Super plots of the number of secondary inclusions in polarized A2EN^{Cas9} and A2EN^{Cas9} *EPS8* KO cells (n = 90 fields of view; unpaired, two-tailed t test). (E) Scatter plots show the number of secondary inclusions in A2EN^{Cas9}or A2EN^{Cas9} *EPS8* KO cells after *primary infections* with *tepP* mutant bacteria (n = 30 fields of view; unpaired, two-tailed t test). (F) Scatter plots show the number of secondary inclusions in *non-confluent* A2EN^{Cas9} and A2EN^{Cas9} *EPS8* KO cells after a primary infection with CTL2-GFP (n = 30 fields of view; unpaired, two-tailed t test).

(G–K) Ectopic expression of TepP is sufficient to promote infection of polarized MDCK cells. (G) Quantification of inclusion per field in polarizing and polarized MDCK cells infected with CTL2 for 20 h (n = 20 fields of view; unpaired, two-tailed t test). (H) MDCK cells expressing mCh or mCh-TepP (not shown) were allowed to polarize and then infected with CTL2-GFP (green) for 20 h. (I) Quantification of inclusions per field in MDCK cells expressing mCh or mCh-TepP and infected with GFP-expressing CTL2 or *tepP* mutants (n = 20 fields of view; unpaired, two-tailed t test). (J) Fluorescence images of MDCK cells expressing mCh or mCh-TepP (magenta), infected with CTL2-GFP (green) for 20 h, and stained for DNA (blue). (K) Quantification of the percent of infected cells expressing mCh or mCh-TepP (n = 20 fields of view; unpaired, two-tailed t test).

(C–F and K) Scatter plots show inclusion number per field, and the bar denotes the median.

(G and I) Box and Whisker plots represent the media and interquartile range ± min and max values.

****$p < 0.0001$.

Please cite this article in press as: Dolat et al., *Chlamydia* repurposes the actin-binding protein EPS8 to disassemble epithelial tight junctions and promote infection, Cell Host & Microbe (2022), https://doi.org/10.1016/j.chom.2022.10.013

CellPress

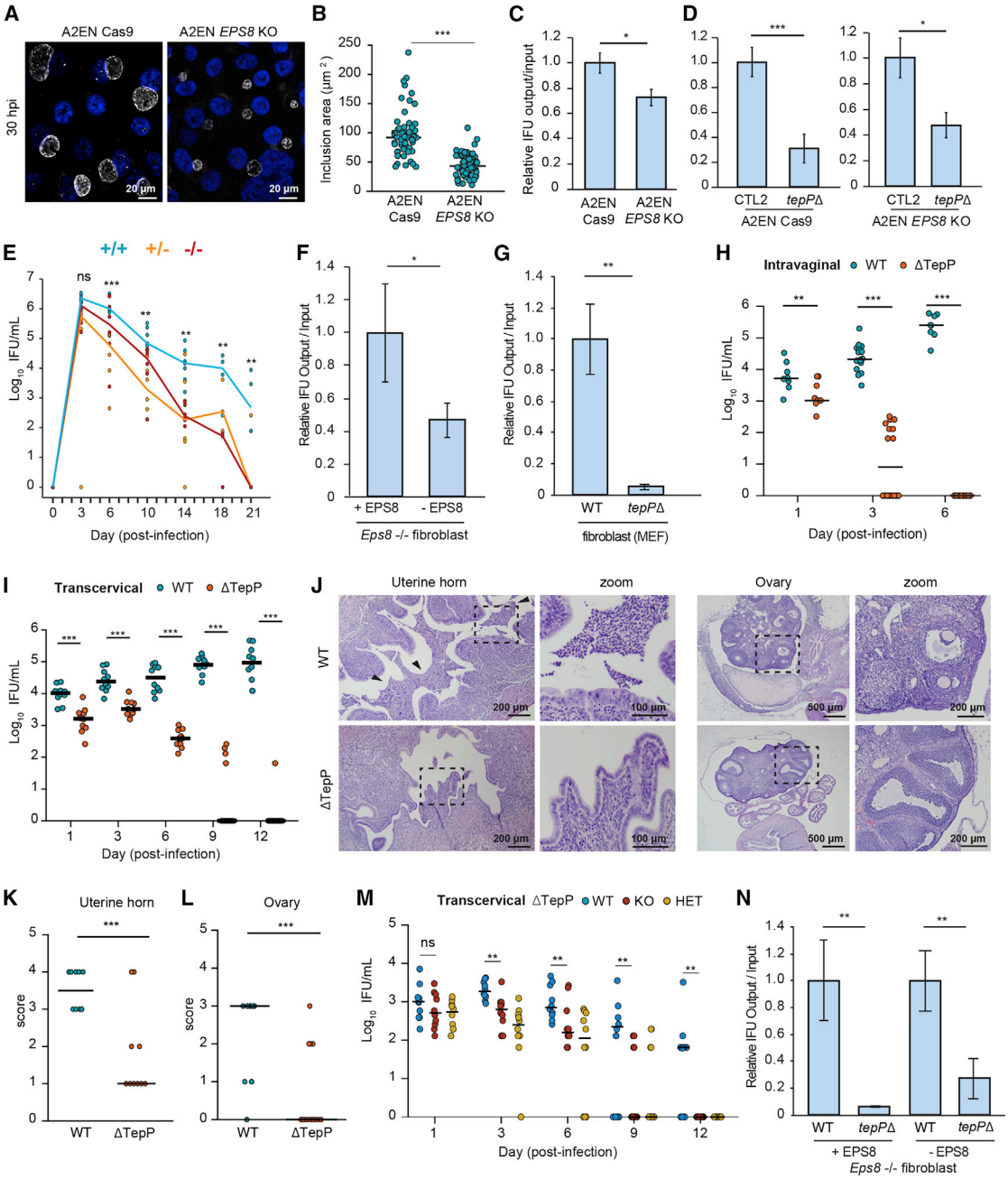

Figure 7. TepP and EPS8 promotes infection in polarized endocervical cells and in the murine female genital tract

(A–D) EPS8 promotes the expansion of CTL2 inclusions and bacterial replication. (A) Confocal images of A2EN^{Cas9} and A2EN^{Cas9} *EPS8* KO cells infected with CTL2 (MOI < 1) for 30 h and immunostained for the inclusion membrane protein Cap1 (white) and DNA (blue). (B) Quantification of inclusion size (n = 59–65 inclusions; unpaired, two-tailed t test). Scatter plots represent the range of inclusion size, and the bar denotes the median. (C) Normalized IFU production of CTL2 in A2EN^{Cas9} and A2EN^{Cas9} *EPS8* KO cells, and (D) CTL2 and *tepP* mutants in A2EN^{Cas9} cells and A2EN^{Cas9} *EPS8* KO cells.

(E) EPS8 promotes C. muridarum infection in vivo. *Eps8*$^{+/+}$ (blue), *Eps8*$^{+/-}$ (yellow), and *Eps8*$^{-/-}$ (red) mouse littermates were infected intravaginally with *C. muridarum*. The number of recoverable IFU were quantified and plotted (n = 6–7 mice for 3–14 dpi, Mann-Whitney U test; n = 3–4 mice for 18, 21 dpi; unpaired, two-tailed t test).

(F and G) EPS8 and TepP promote C. muridarum replication. (F) Normalized production of *C. muridarum* IFUs after replication in *Eps8*$^{-/-}$ fibroblasts stably expressing EPS8 (+EPS8) or an empty vector (−EPS8). (G) Normalized IFU production of *C. muridarum* wild-type and *tepP* mutant bacteria in mouse fibroblasts.

(H–L) TepP promotes C. muridarum colonization and pathology in the upper genital tract. (H) Mice were infected intravaginally with *C. muridarum* wild-type or *tepP* mutant bacteria and swabbed at the indicated day. The number of recoverable IFU were quantified (n = 8–16 mice; Mann-Whitney U test). (I) Mice were infected transcervically with *C. muridarum* wild-type or *tepP* mutant bacteria and swabbed at the indicated day. The number of recoverable IFU were quantified (n = 10 mice; Mann-Whitney U test). (J) Hematoxylin and eosin-stained sections of the uterine horns and ovaries from mice infected with *C. muridarum* wild-type or *tepP* mutant bacteria at 14 day post-infection. Arrows denote increased levels of cellular infiltrates. (K and L) Scatter plots of acute pathology scores of the uterine

(legend continued on next page)

assistance with microscopy; Dr. Terry Lechler for the ZO-1 GFP mouse line; Dr. Erik Soderblom and Dr. Arthur Moseley at the Duke Proteomic and Metabolomics Core Facility, Gary Kucera and Cheryl Bock at the Duke Rodent Genetic Engineering Molecular Services Team, Dr. So Young Kim at the Duke RNAi Screening Facility, Dr. Michelle Plue at Duke Shared Materials Instrumentation Facility for assistance with electron microscopy; and Dr. Jeffrey Everitt for assistance with pathological analysis. We also thank Dr. David Tobin and Dr. Carolyn Coyne for critical comments on the manuscript and members of the Valdivia lab for feedback on this project. This work was funded by NIH grants AI134891 (R.H.V.) and AI138372 (L.D.).

AUTHOR CONTRIBUTIONS

L.D., V.K.C., and R.H.V. designed experiments; L.D. and V.K.C. performed experiments; L.D., V.K.C., Y.-S.C., M.S., E.P.S., and O.K. generated reagents; L.D. and R.H.V. wrote the paper.

DECLARATION OF INTERESTS

R.H.V. is a founder of Bloom Sciences (San Diego, CA), which is a microbiome therapeutics company. The current manuscript is unrelated to the work performed with Bloom Sciences.

INCLUSION AND DIVERSITY

This work was performed by a team of individuals with diverse background and life experiences. We support inclusive and equitable conduct of research.

Received: February 28, 2022
Revised: August 8, 2022
Accepted: October 21, 2022
Published: November 16, 2022

REFERENCES

1. WHO (2018). Report on Global Sexually Transmitted Infection Surveillance (World Health Organization).
2. Haggerty, C.L., Gottlieb, S.L., Taylor, B.D., Low, N., Xu, F., and Ness, R.B. (2010). Risk of sequelae after *Chlamydia trachomatis* genital infection in women. J. Infect. Dis. *201*, S134–S155.
3. Garcia, M.A., Nelson, W.J., and Chavez, N. (2018). Cell-cell junctions organize structural and signaling networks. Cold Spring Harb. Perspect. Biol. *10*.
4. Zihni, C., Mills, C., Matter, K., and Balda, M.S. (2016). Tight junctions: from simple barriers to multifunctional molecular gates. Nat. Rev. Mol. Cell Biol. *17*, 564–580.
5. Guttman, J.A., and Finlay, B.B. (2009). Tight junctions as targets of infectious agents. Biochim. Biophys. Acta *1788*, 832–841.
6. Paradis, T., Bègue, H., Basmaciyan, L., Dalle, F., and Bon, F. (2021). Tight junctions as a key for pathogens invasion in intestinal epithelial cells. Int. J. Mol. Sci. *22*, 2506.
7. Dolat, L., and Valdivia, R.H. (2021). An endometrial organoid model of interactions between *Chlamydia* and epithelial and immune cells. J. Cell Sci. *134*, jcs252403.
8. Kessler, M., Zielecki, J., Thieck, O., Mollenkopf, H.-J., Fotopoulou, C., and Meyer, T.F. (2012). *Chlamydia trachomatis* disturbs epithelial tissue homeostasis in fallopian tubes via paracrine Wnt signaling. Am. J. Pathol. *180*, 186–198.
9. Abdelrahman, Y.M., and Belland, R.J. (2005). The chlamydial developmental cycle. FEMS Microbiol. Rev. *29*, 949–959.
10. Elwell, C.A., Ceesay, A., Kim, J.H., Kalman, D., and Engel, J.N. (2008). RNA interference screen identifies Abl kinase and PDGFR signaling in *Chlamydia trachomatis* entry. PLoS Pathog. *4*, e1000021.
11. Patel, A.L., Chen, X., Wood, S.T., Stuart, E.S., Arcaro, K.F., Molina, D.P., Petrovic, S., Furdui, C.M., and Tsang, A.W. (2014). Activation of epidermal growth factor receptor is required for *Chlamydia trachomatis* development. BMC Microbiol. *14*, 277.
12. Rosmarin, D.M., Carette, J.E., Olive, A.J., Starnbach, M.N., Brummelkamp, T.R., and Ploegh, H.L. (2012). Attachment of *Chlamydia trachomatis* L2 to host cells requires sulfation. Proc. Natl. Acad. Sci. USA *109*, 10059–10064.
13. Stallmann, S., and Hegemann, J.H. (2016). The *Chlamydia trachomatis* Ctad1 invasin exploits the human integrin β1 receptor for host cell entry. Cell Microbiol. *18*, 761–775.
14. Subbarayal, P., Karunakaran, K., Winkler, A.-C., Rother, M., Gonzalez, E., Meyer, T.F., and Rudel, T. (2015). EphrinA2 receptor (EphA2) is an invasion and intracellular signaling receptor for *Chlamydia trachomatis*. PLoS Pathog. *11*, e1004846.
15. Elwell, C., Mirrashidi, K., and Engel, J. (2016). *Chlamydia* cell biology and pathogenesis. Nat. Rev. Microbiol. *14*, 385–400.
16. Al-Zeer, M.A., Al-Younes, H.M., Kerr, M., Abu-Lubad, M., Gonzalez, E., Brinkmann, V., and Meyer, T.F. (2014). *Chlamydia trachomatis* remodels stable microtubules to coordinate Golgi stack recruitment to the chlamydial inclusion surface. Mol. Microbiol. *94*, 1285–1297.
17. Mital, J., Lutter, E.I., Barger, A.C., Dooley, C.A., and Hackstadt, T. (2015). *Chlamydia trachomatis* inclusion membrane protein CT850 interacts with the dynein light chain DYNLT1 (Tctex1). Biochem. Biophys. Res. Commun. *462*, 165–170.
18. Hybiske, K., and Stephens, R.S. (2007). Mechanisms of host cell exit by the intracellular bacterium *Chlamydia*. Proc. Natl. Acad. Sci. USA *104*, 11430–11435.
19. Brinkworth, A.J., Malcolm, D.S., Pedrosa, A.T., Roguska, K., Shahbazian, S., Graham, J.E., Hayward, R.D., and Carabeo, R.A. (2011). *Chlamydia trachomatis* Slc1 is a type III secretion chaperone that enhances the translocation of its invasion effector substrate TARP. Mol. Microbiol. *82*, 131–144.
20. Chen, Y.-S., Bastidas, R.J., Saka, H.A., Carpenter, V.K., Richards, K.L., Plano, G.V., and Valdivia, R.H. (2014). The *Chlamydia trachomatis* type III secretion chaperone Slc1 engages multiple early effectors, including TepP, a tyrosine-phosphorylated protein required for the recruitment of CrkI-II to nascent inclusions and innate immune signaling. PLoS Pathog. *10*, e1003954.
21. Jewett, T.J., Fischer, E.R., Mead, D.J., and Hackstadt, T. (2006). Chlamydial TARP is a bacterial nucleator of actin. Proc. Natl. Acad. Sci. USA *103*, 15599–15604.
22. Keb, G., Hayman, R., and Fields, K.A. (2018). Floxed-cassette allelic exchange mutagenesis enables markerless gene deletion in *Chlamydia trachomatis* and can reverse cassette-induced polar effects. J. Bacteriol. *200*, e00479-18.
23. Faris, R., McCullough, A., Andersen, S.E., Moninger, T.O., and Weber, M.M. (2020). The *Chlamydia trachomatis* secreted effector TmeA hijacks the N-WASP-ARP2/3 actin remodeling axis to facilitate cellular invasion. PLoS Pathog. *16*, e1008878.
24. Keb, G., Ferrell, J., Scanlon, K.R., Jewett, T.J., and Fields, K.A. (2021). *Chlamydia trachomatis* TmeA directly activates N-WASP To promote actin

horns and ovaries (n = 5 mice; unpaired, two-tailed t test). Data represent scores of individual uterine horns and ovaries, and the line denotes the median. (M) *Eps8*$^{+/+}$, *Eps8*$^{+/-}$, and *Eps8*$^{-/-}$ mouse littermates were infected transcervically with *C. muridarum tepP* mutant bacteria and swabbed at the indicated day. The number of recoverable IFU were quantified (n = 10 mice; Mann-Whitney U test). (N) Normalized IFU production of *C. muridarum* wild-type and *tepP* mutant bacteria in *Eps8*$^{-/-}$ fibroblasts complemented with EPS8 (+EPS8) or an empty vector (−EPS8).
All bar graphs represent the mean ± SD (n = 3 independent experiments; unpaired, two-tailed t test).
*p < 0.05, **p < 0.01, ***p < 0.001, ****p < 0.0001.

polymerization and functions synergistically with TarP during invasion. mBio *12*, e02861-20.

25. Lane, B.J., Mutchler, C., Al Khodor, S., Grieshaber, S.S., and Carabeo, R.A. (2008). Chlamydial entry involves TARP binding of guanine nucleotide exchange factors. PLoS Pathog. *4*, e1000014.
26. Carpenter, V., Chen, Y.-S., Dolat, L., and Valdivia, R.H. (2017). The effector TepP mediates recruitment and activation of phosphoinositide 3-kinase on early *Chlamydia trachomatis* vacuoles. mSphere *2*, e00207-17.
27. Saka, H.A., Thompson, J.W., Chen, Y.-S., Kumar, Y., Dubois, L.G., Moseley, M.A., and Valdivia, R.H. (2011). Quantitative proteomics reveals metabolic and pathogenic properties of *Chlamydia trachomatis* developmental forms. Mol. Microbiol. *82*, 1185–1203.
28. Backert, S., and Selbach, M. (2005). Tyrosine-phosphorylated bacterial effector proteins: the enemies within. Trends Microbiol. *13*, 476–484.
29. Gruenheid, S., DeVinney, R., Bladt, F., Goosney, D., Gelkop, S., Gish, G.D., Pawson, T., and Finlay, B.B. (2001). Enteropathogenic *E. coli* Tir binds Nck to initiate actin pedestal formation in host cells. Nat. Cell Biol. *3*, 856–859.
30. Higashi, H., Tsutsumi, R., Muto, S., Sugiyama, T., Azuma, T., Asaka, M., and Hatakeyama, M. (2002). SHP-2 tyrosine phosphatase as an intracellular target of *Helicobacter pylori* CagA protein. Science *295*, 683–686.
31. Sorg, I., Schmutz, C., Lu, Y.-Y., Fromm, K., Siewert, L.K., Bögli, A., Strack, K., Harms, A., and Dehio, C. (2020). A *Bartonella* effector acts as signaling hub for intrinsic STAT3 activation to trigger anti-inflammatory responses. Cell Host Microbe *27*, 476–485.e7.
32. Postema, M.M., Grega-Larson, N.E., Neininger, A.C., and Tyska, M.J. (2018). IRTKS (BAIAP2L1) elongates epithelial microvilli using EPS8-dependent and independent mechanisms. Curr. Biol. *28*, 2876–2888.e4.
33. Vaggi, F., Disanza, A., Milanesi, F., Di Fiore, P.P., Menna, E., Matteoli, M., Gov, N.S., Scita, G., and Ciliberto, A. (2011). The Eps8/IRSp53/VASP network differentially controls actin capping and bundling in filopodia formation. PLoS Comput. Biol. *7*, e1002088.
34. Zampini, V., Rüttiger, L., Johnson, S.L., Franz, C., Furness, D.N., Waldhaus, J., Xiong, H., Hackney, C.M., Holley, M.C., Offenhauser, N., et al. (2011). Eps8 regulates hair bundle length and functional maturation of mammalian auditory hair cells. PLoS Biol. *9*, e1001048.
35. Ghosh, S., Ruelke, E.A., Ferrell, J.C., Bodero, M.D., Fields, K.A., and Jewett, T.J. (2020). Fluorescence-reported allelic exchange mutagenesis-mediated gene deletion indicates a requirement for *Chlamydia trachomatis* Tarp during *in vivo* infectivity and reveals a specific role for the C terminus during cellular invasion. Infect. Immun. *88*, e00841-19.
36. Thwaites, T., Nogueira, A.T., Campeotto, I., Silva, A.P., Grieshaber, S.S., and Carabeo, R.A. (2014). The *Chlamydia* effector TarP mimics the mammalian leucine-aspartic acid motif of paxillin to subvert the focal adhesion kinase during invasion. J. Biol. Chem. *289*, 30426–30442.
37. Lanzetti, L., Rybin, V., Malabarba, M.G., Christoforidis, S., Scita, G., Zerial, M., and Di Fiore, P.P. (2000). The Eps8 protein coordinates EGF receptor signalling through Rac and trafficking through Rab5. Nature *408*, 374–377.
38. Scita, G., Nordstrom, J., Carbone, R., Tenca, P., Giardina, G., Gutkind, S., Bjarnegård, M., Betsholtz, C., and Di Fiore, P.P. (1999). EPS8 and E3B1 transduce signals from Ras to Rac. Nature *401*, 290–293.
39. Disanza, A., Carlier, M.-F., Stradal, T.E.B., Didry, D., Frittoli, E., Confalonieri, S., Croce, A., Wehland, J., Di Fiore, P.P., and Scita, G. (2004). Eps8 controls actin-based motility by capping the barbed ends of actin filaments. Nat. Cell Biol. *6*, 1180–1188.
40. Hertzog, M., Milanesi, F., Hazelwood, L., Disanza, A., Liu, H., Perlade, E., Malabarba, M.G., Pasqualato, S., Maiolica, A., Confalonieri, S., et al. (2010). Molecular basis for the dual function of Eps8 on actin dynamics: bundling and capping. PLoS Biol. *8*, e1000387.
41. Zwaenepoel, I., Naba, A., Da Cunha, M.M.L., Del Maestro, L., Formstecher, E., Louvard, D., and Arpin, M. (2012). Ezrin regulates microvillus morphogenesis by promoting distinct activities of Eps8 proteins. Mol. Biol. Cell *23*, 1080–1094.
42. Maa, M.-C., Lai, J.-R., Lin, R.-W., and Leu, T.-H. (1999). Enhancement of tyrosyl phosphorylation and protein expression of eps8 by v-Src. Biochim. Biophys. Acta *1450*, 341–351.
43. Moore, E.R., Fischer, E.R., Mead, D.J., and Hackstadt, T. (2008). The chlamydial inclusion preferentially intercepts basolaterally directed sphingomyelin-containing exocytic vacuoles. Traffic *9*, 2130–2140.
44. Coers, J., Starnbach, M.N., and Howard, J.C. (2009). Modeling infectious disease in mice: co-adaptation and the role of host-specific IFNF067 responses. PLoS Pathog. *5*, e1000333.
45. Prozialeck, W.C., Fay, M.J., Lamar, P.C., Pearson, C.A., Sigar, I., and Ramsey, K.H. (2002). *Chlamydia trachomatis* disrupts *N*-cadherin-dependent cell-cell junctions and sequesters F062-catenin in human cervical epithelial cells. Infect. Immun. *70*, 2605–2613.
46. Kierbel, A., Gassama-Diagne, A., Rocha, C., Radoshevich, L., Olson, J., Mostov, K., and Engel, J. (2007). *Pseudomonas aeruginosa* exploits a PIP3-dependent pathway to transform apical into basolateral membrane. J. Cell Biol. *177*, 21–27.
47. Coyne, C.B., and Bergelson, J.M. (2006). Virus-induced Abl and Fyn kinase signals permit Coxsackie virus entry through epithelial tight junctions. Cell *124*, 119–131.
48. Hayashi, K., Hayashi, M., Boutin, E., Cunha, G.R., Bernfield, M., and Trelstad, R.L. (1988). Hormonal modification of epithelial differentiation and expression of cell surface heparan sulfate proteoglycan in the mouse vaginal epithelium. An immunohistochemical and electron microscopic study. Lab. Invest. *58*, 68–76.
49. Inki, P. (1997). Expression of syndecan-1 in female reproductive tract tissues and cultured keratinocytes. Mol. Hum. Reprod. *3*, 299–305.
50. Zhang, J.P., and Stephens, R.S. (1992). Mechanism of *C. trachomatis* attachment to eukaryotic host cells. Cell *69*, 861–869.
51. Birkelund, S., Johnsen, H., and Christiansen, G. (1994). *Chlamydia trachomatis* serovar L2 induces protein tyrosine phosphorylation during uptake by HeLa cells. Infect. Immun. *62*, 4900–4908.
52. Fawaz, F.S., van Ooij, C., Homola, E., Mutka, S.C., and Engel, J.N. (1997). Infection with *Chlamydia trachomatis* alters the tyrosine phosphorylation and/or localization of several host cell proteins including cortactin. Infect. Immun. *65*, 5301–5308.
53. Clifton, D.R., Fields, K.A., Grieshaber, S.S., Dooley, C.A., Fischer, E.R., Mead, D.J., Carabeo, R.A., and Hackstadt, T. (2004). A chlamydial type III translocated protein is tyrosine-phosphorylated at the site of entry and associated with recruitment of actin. Proc. Natl. Acad. Sci. USA *101*, 10166–10171.
54. Offenhäuser, N., Borgonovo, A., Disanza, A., Romano, P., Ponzanelli, I., Iannolo, G., Di Fiore, P.P., and Scita, G. (2004). The eps8 family of proteins links growth factor stimulation to actin reorganization generating functional redundancy in the Ras/Rac pathway. Mol. Biol. Cell *15*, 91–98.
55. Cunningham, D.L., Creese, A.J., Auciello, G., Sweet, S.M.M., Tatar, T., Rappoport, J.Z., Grant, M.M., and Heath, J.K. (2013). Novel binding partners and differentially regulated phosphorylation sites clarify Eps8 as a multi-functional adaptor. PLoS One *8*, e61513.
56. Shahoumi, L.A., Khodadadi, H., Bensreti, H., Baban, B., and Yeudall, W.A. (2020). EPS8 phosphorylation by Src modulates its oncogenic functions. Br. J. Cancer *123*, 1078–1088.
57. Fredriksson, K., Van Itallie, C.M., Aponte, A., Gucek, M., Tietgens, A.J., and Anderson, J.M. (2015). Proteomic analysis of proteins surrounding occludin and claudin-4 reveals their proximity to signaling and trafficking networks. PLoS One *10*, e0117074.
58. Giampietro, C. (2016). VE-cadherin complex plasticity: EPS8 and YAP play relay at adherens junctions. Tissue Barriers *4*, e1232024.
59. Shah, A.A., Schripsema, J.H., Imtiaz, M.T., Sigar, I.M., Kasimos, J., Matos, P.G., Inouye, S., and Ramsey, K.H. (2005). Histopathologic changes related to fibrotic oviduct occlusion after genital tract infection of mice with *Chlamydia muridarum*. Sex. Transm. Dis. *32*, 49–56.
60. Nagarajan, U.M., Prantner, D., Sikes, J.D., Andrews, C.W., Goodwin, A.M., Nagarajan, S., and Darville, T. (2008). Type I interferon signaling

exacerbates *Chlamydia muridarum* genital infection in a murine model. Infect. Immun. *76*, 4642–4648.

61. Scidmore-Carlson, M.A., Shaw, E.I., Dooley, C.A., Fischer, E.R., and Hackstadt, T. (1999). Identification and characterization of a *Chlamydia trachomatis* early operon encoding four novel inclusion membrane proteins. Mol. Microbiol. *33*, 753–765.
62. Delevoye, C., Nilges, M., Dehoux, P., Paumet, F., Perrinet, S., Dautry-Varsat, A., and Subtil, A. (2008). SNARE protein mimicry by an intracellular bacterium. PLoS Pathog. *4*, e1000022.
63. Huston, W.M., Theodoropoulos, C., Mathews, S.A., and Timms, P. (2008). Chlamydia trachomatis responds to heat shock, penicillin induced persistence, and IFN-gamma persistence by altering levels of the extracytoplasmic stress response protease HtrA. BMC microbiology *8*, 190. https://doi.org/10.1186/1471-2180-8-190.
64. Buckner, L.R., Lewis, M.E., Greene, S.J., Foster, T.P., and Quayle, A.J. (2013). *Chlamydia trachomatis* infection results in a modest pro-inflammatory cytokine response and a decrease in T cell chemokine secretion in human polarized endocervical epithelial cells. Cytokine *63*, 151–165.
65. Werner, A., Disanza, A., Reifenberger, N., Habeck, G., Becker, J., Calabrese, M., Urlaub, H., Lorenz, H., Schulman, B., Scita, G., and Melchior, F. (2013). SCFFbxw5 mediates transient degradation of actin remodeller Eps8 to allow proper mitotic progression. Nat. Cell Biol. *15*, 179–188.
66. Foote, H.P., Sumigray, K.D., and Lechler, T. (2013). FRAP analysis reveals stabilization of adhesion structures in the epidermis compared to cultured keratinocytes. PLoS One *8*, e71491.
67. Agaisse, H., and Derré, I. (2013). A *C. trachomatis* cloning vector and the generation of *C. trachomatis* strains expressing fluorescent proteins under the control of a *C. trachomatis* promoter. PLoS One *8*, e57090.
68. Sixt, B.S., Bastidas, R.J., Finethy, R., Baxter, R.M., Carpenter, V.K., Kroemer, G., Coers, J., and Valdivia, R.H. (2017). The *Chlamydia trachomatis* inclusion membrane protein CpoS counteracts STING-mediated cellular surveillance and suicide programs. Cell Host Microbe *21*, 113–121.
69. Lowden, N.M., Yeruva, L., Johnson, C.M., Bowlin, A.K., and Fisher, D.J. (2015). Use of aminoglycoside 3′ adenyltransferase as a selection marker for *Chlamydia trachomatis* intron-mutagenesis and *in vivo* intron stability. BMC Res. Notes *8*, 570.
70. Johnson, C.M., and Fisher, D.J. (2013). Site-specific, insertional inactivation of incA in Chlamydia trachomatis using a group II intron. PloS one *8*, e83989. https://doi.org/10.1371/journal.pone.0083989.
71. Cortina, M.E., Ende, R.J., Bishop, R.C., Bayne, C., and Derré, I. (2019). *Chlamydia trachomatis* and *Chlamydia muridarum* spectinomycin resistant vectors and a transcriptional fluorescent reporter to monitor conversion from replicative to infectious bacteria. PLoS One *14*, e0217753.
72. Wang, Y., Cutcliffe, L.T., Skilton, R.J., Ramsey, K.H., Thomson, N.R., and Clarke, I.N. (2014). The genetic basis of plasmid tropism between *Chlamydia trachomatis* and *Chlamydia muridarum*. Pathog. Dis. *72*, 19–23.
73. Schindelin, J., Arganda-Carreras, I., Frise, E., Kaynig, V., Longair, M., Pietzsch, T., Preibisch, S., Rueden, C., Saalfeld, S., Schmid, B., et al. (2012). Fiji: an open-source platform for biological-image analysis. Nat. Methods *9*, 676–682.
74. Miyoshi, H., and Stappenbeck, T.S. (2013). *In vitro* expansion and genetic modification of gastrointestinal stem cells in spheroid culture. Nat. Protoc. *8*, 2471–2482.
75. Poston, T.B., O'Connell, C.M., Girardi, J., Sullivan, J.E., Nagarajan, U.M., Marinov, A., Scurlock, A.M., and Darville, T. (2018). T cell-independent gamma interferon and B cells cooperate to prevent mortality associated with disseminated *Chlamydia muridarum* genital tract infection. Infect. Immun. *86*, e00143-18.
76. Concordet, J.-P., and Haeussler, M. (2018). CRISPOR: intuitive guide selection for CRISPR/Cas9 genome editing experiments and screens. Nucleic Acids Res. *46*, W242–W245.
77. Modzelewski, A.J., Chen, S., Willis, B.J., Lloyd, K.C.K., Wood, J.A., and He, L. (2018). Efficient mouse genome engineering by CRISPR-EZ technology. Nat. Protoc. *13*, 1253–1274.
78. Raudvere, U., Kolberg, L., Kuzmin, I., Arak, T., Adler, P., Peterson, H., and Vilo, J. (2019). g:Profiler: a web server for functional enrichment analysis and conversions of gene lists (2019 update). Nucleic Acids Res. *47*, W191–W198.

Please cite this article in press as: Dolat et al., *Chlamydia* repurposes the actin-binding protein EPS8 to disassemble epithelial tight junctions and promote infection, Cell Host & Microbe (2022), https://doi.org/10.1016/j.chom.2022.10.013

CellPress

STAR★METHODS

KEY RESOURCES TABLE

REAGENT or RESOURCE	SOURCE	IDENTIFIER
Antibodies		
Rabbit anti-EPS8	Abcam	Cat# 96144; RRID:AB_10678966
Mouse anti-EPS8	BD Biosciences	Cat# 610143; RRID:AB_397544
Mouse anti-phospho-Tyr	Cell Signaling Technology	Cat# 9411S;RRID:AB_331228
Mouse anti-MOMP	Santa Cruz Biotechnology	Cat# Sc-57678;RRID:AB_1119779
Mouse anti-beta-catenin	BD Biosciences	Cat# 610154;RRID:AB_397555
Rabbit anti-ZO-1	Cell Signaling Technology	Cat# 8193S;RRID:AB_10898025
Rabbit anti-E-cadherin	Cell Signaling Technology	Cat# 3195; RRID:AB_2291471
Rabbit anti-Slc1	Chen et al.[20]	N/A
Rabbit anti-TepP	Chen et al.[20]	N/A
Rabbit anti-IncG	Scidmore-Carlson et al.[61]	N/A
Rabbit anti-Cap1	Delevoye et al.[62]	N/A
Rabbit anti-HtrA	Huston et al.[63]	N/A
Mouse anti-LPS	Dan Rockey, Oregon State University	N/A
Rabbit anti-GFP	Thermo Fisher Scientific	Cat# A11122;RRID:AB_221569
Rabbit anti-DsRed	Takara Bio	Cat# 632496;RRID:AB_10013483
Mouse anti-alpha-tubulin	Sigma-Aldrich	Cat# T5168;RRID:AB_477579
Mouse anti-beta-actin	Sigma-Aldrich	Cat# A2228;RRID:AB_476697
Rabbit PTMScan phospho-Tyr	Cell Signaling Technology	Cat# 8803
Goat anti-Mouse IgG 680	LI-COR Biosciences	Cat# 926-68020;RRID:AB_10706161
Goat anti-Rabbit IgG 680	LI-COR Biosciences	Cat# 926-68021;RRID:AB_10706309
Goat anti-Mouse IgG 800	LI-COR Biosciences	Cat# 926-32210;RRID:AB_621842
Goat anti-Rabbit IgG 800	LI-COR Biosciences	Cat# 926-32211;RRID:AB_621843
Goat anti-mouse 488	Thermo Fisher Scientific	Cat# A-11029;RRID:AB_2534088
Goat anti-rabbit 488	Thermo Fisher Scientific	Cat# A-11008;RRID:AB_143165
Goat anti-mouse 555	Thermo Fisher Scientific	Cat# A-21422;RRID:AB_2535844
Goat anti-rabbit 555	Thermo Fisher Scientific	Cat# A-21428;RRID:AB_2535849
Goat anti-rabbit 647	Thermo Fisher Scientific	Cat# A-21236;RRID:AB_2535805
GFP-Trap	ChromoTek	Cat# GTMA-20;RRID:AB_2631358
Chemicals, peptides, and recombinant proteins		
DMSO	Sigma-Aldrich	Cat# D2438
Latrunculin A	Sigma-Aldrich	Cat# I5163
PP2	Sigma-Aldrich	Cat# P0042
Acti-stain 488	Cytoskeleton	Cat# PHDG1-A
Acti-stain 555	Cytoskeleton	Cat# PHDH1-A
SiR-Actin	Cytoskeleton	Cat# CY-SC001
16% paraformaldehyde	Electron Microscopy Services	Cat# 15710
Triton X-100	EMD Millipore	Cat# TX1568-1
Hoechst	Thermo Fisher Scientific	Cat# 62249
Vectashield	Vector Labs	Cat# H-1000
FluorSave Reagent	EMD Millipore	Cat# 345789
Tannic Acid	Electron Microscopy Services	Cat# 21700
Sodium cacodylate trihydrate	Electron Microscopy Services	Cat# 12300
Osmium Tetroxide	Electron Microscopy Services	Cat# 19152
Uranyl acetate	Electron Microscopy Services	Cat# 22400

(*Continued on next page*)

Please cite this article in press as: Dolat et al., *Chlamydia* repurposes the actin-binding protein EPS8 to disassemble epithelial tight junctions and promote infection, Cell Host & Microbe (2022), https://doi.org/10.1016/j.chom.2022.10.013

Continued

REAGENT or RESOURCE	SOURCE	IDENTIFIER
K3Fe(CN)6	Electron Microscopy Services	Cat# 20150
Malachite green	Electron Microscopy Services	Cat# 18100
Ammonium chloride	Sigma-Aldrich	Cat# A-5666
jetPRIME Transfection Reagent	PolyPlus	Cat# 89129-924
Texas-Red Dextran (3 kDa)	Thermo Fisher Scientific	Cat# D3329
Spectinomycin	Millipore	Cat# 567570
Penicillin	Sigma-Aldrich	Cat# P3032-10MU
Gentamicin	Gibco	Cat# 15750060
Type I collagen	Invitrogen	Cat# A1048301
cOmplete, EDTA_free protease inhibitor	Millipore Sigma	Cat# 11836170001
Halt phosphatase inhibitor	Thermo Fisher Scientific	Cat# 78428
BSA (Fraction V)	Equitech-Bio	Cat# BAC61-1000
Tween-20	Sigma-Aldrich	Cat# P9416
Collagenase A	Sigma-Alddrich	Cat# 10103578001
Matrigel	Corning	Cat# 356231
EGF	STEMCELL Technologies	Cat# 78016.1
Experimental models: Cell lines		
HeLa	ATCC	CCL-2;RRID:CVCL_0030
Vero	ATCC	CCL-81;RRID:CVCL_0059
A2EN	Buckner et al.[64]	N/A
A2EN Cas9	This paper	N/A
A2EN *EPS8* KO	This paper	N/A
SYF	ATCC	CRL-2459
SYF + c-Src	ATCC	CRL-2498
MEF	ATCC	CF-1;RRID:CVCL_5251
293T	ATCC	CRL-3216
MDCK-1	ATCC	CCL-34;RRID:CVCL_0422
L-WRN	ATCC	CRL-3276
Eps8 -/- pBABE EPS8-GFP	Werner et al.[65]	N/A
Eps8 -/- pBABE	Werner et al.[65]	N/A
Experimental models: Mice		
C57BL/6J	Jackson Laboratory	000664
Eps8 -/-	This paper	N/A
ZO-1 GFP	Foote et al.[66]	N/A
Experimental models: Bacterial strains		
CTL2 434/Bu	ATCC	VR-902B
CTD UW-3/Cx	ATCC	VR-885
CTL2-p2TK2 GFP	Agaisse and Derré[67]	N/A
CTL2-p2TK2 mCherry	Agaisse and Derré[67]	N/A
CTL2 *tepP*::GII *aadA*	Dolat and Valdivia[7]	N/A
CTL2 *tepP*::GII *aadA* + pTepP	Dolat and Valdivia[7]	N/A
CTL2 *tepP*::GII *aadA* + pVector	Dolat and Valdivia[7]	N/A
CTL2 *tmeA*::GII *aadA*	This paper	N/A
CTL2 *tmeB*::GII *aadA*	This paper	N/A
CTL2 *tarP*::bla	Ghosh et al.[35]	N/A
CTL2 M923-p2TK2 mCherry	Sixt et al.[68]	N/A
CTL2-M062G1 [$tepP^{Q103*}$] + pTepP	Carpenter et al.[26]	N/A
CTL2-M062G1 [$tepP^{Q103*}$] + pVector	Carpenter et al.[26]	N/A
CTL2 *tepP*::GII *aadA* p2TK2-GFP	Dolat and Valdivia[7]	N/A
CTL2 *tmeA*::GII *aadA* p2TK2-GFP	This paper	N/A

(*Continued on next page*)

Please cite this article in press as: Dolat et al., *Chlamydia* repurposes the actin-binding protein EPS8 to disassemble epithelial tight junctions and promote infection, Cell Host & Microbe (2022), https://doi.org/10.1016/j.chom.2022.10.013

Continued

REAGENT or RESOURCE	SOURCE	IDENTIFIER
CTL2 *tmeB*::GII *aadA* p2TK2-GFP	This paper	N/A
C. muridarum CM006-GFP	Dolat and Valdivia[7]	N/A
C. muridarum CM001-mCherry	This paper	N/A
C. muridarum MoPn	Catherine O'Connell (UNC-Chapel Hill)	N/A
C. muridarum MoPn *tepP* :: GII *bla*	This paper	N/A
Oligonucleotides		
See Table S2		N/A
Recombinant DNA		
C1-mCherry-TepP	This paper	N/A
EGFP-EPS8	Postema et al.[32]	N/A
EGFP-EPS8-4xYF	This paper	N/A
EGFP-EPS8-ΔABD	This paper	N/A
EGFP-EPS8-SH3+ABD	This paper	N/A
p2TK2-SW2-GFP	Agaisse and Derré[67]	N/A
pDFTT3::*aadA*	Lowden et al.[69]	N/A
pDFTT3::bla	Johnson and Fisher[70]	N/A
pDFTT3::*aadA*-CTL0063-280	This paper	N/A
pDFTT3::*aadA*-CTL0064-187	This paper	N/A
pDFTT3::*bla*-TC0268-438	This paper	N/A
p2TK2-spec-Nigg-mCherry	Cortina et al.[71]	N/A
pSW2NiggCDS2	Wang et al.[72]	N/A
psPAX2	Dr. Didier Trono	Addgene #12260;RRID:Addgene_12260
pMD2.G	Dr. Dider Trono	Addgene #12259;RRID_Addgene_12259
Software and algorithms		
NIS Elements	Nikon Instruments	N/A
R Studio	N/A	N/A
ImageJ	Schindelin et al.[73]	N/A
Excel	Microsoft	N/A

RESOURCE AVAILABILITY

Lead Contact

Further information and requests for resources and reagents should be directed to the lead contact, Raphael Valdivia (raphael.valdivia@duke.edu).

Materials availability

Bacterial strains, plasmids and cell lines will be made available on request.

Data and code availability

- Phospho-proteomic datasets were deposited to MassIVE and will be available on the date of publication.
- This paper does not report original code.
- Any additional information required to reanalyze the data reported in this work paper is available from the lead contact upon request

EXPERIMENTAL MODEL AND SUBJECT DETAILS

Cell lines and conditioned medium

Vero (CCL-81), HeLa (CCL-2), SYF (CRL-2459), SYF + c-Src (CRL-2498), MEF (CF-1), 293T (CRL-3216), MDCK-I (CCL-34) cells were purchased from ATCC and cultured in Dulbecco's Modified Eagle's Medium (DMEM; Gibco) containing 10% fetal bovine serum (FBS; Sigma-Aldrich). A2EN endocervical epithelial cells were a gift from Dr. Alison Quayle (Louisiana State University Health Sciences Center) and cultured in keratinocyte serum-free media (GIBCO) containing 10% FBS and growth factors according to the manufacturer. Eps8$^{-/-}$

fibroblasts stably expressing EPS8 or an empty vector were a gift from Dr. Giorgio Scita (The Firc Institute of Molecular Oncology, Milan, Italy). L-WRN cells were purchased from ATCC (CRL-3276) and cultured in DMEM containing 0.5 mg/mL geneticin (Gibco) and 0.5 mg/mL hygromycin B (Thermo Fisher Scientific) at 37°C with 5% CO2. Conditioned medium was generated as previously described.[74]

Chlamydia strains and propagation

C. trachomatis L2/434/Bu (CTL2; ATCC VR-902B), Serovar D (Gift from Dr. Michael Starnbach), the genetically modified *C. trachomatis* L2 *tarp* (Gift from Dr. Ken Fields), *tepP*,[7] *tmeA*, *tmeB*, M923,[68] and the *C. trachomatis* L2 strains expressing p2TK2-GFP or p2TK2-mCherry were propagated in Vero cells, harvested by water lysis at 44-48 h post-infection, sonicated, diluted in SPG (sucrose-phosphate-glutamate) buffer to 1x concentration (75 g/L sucrose, 0.5 g/L KH4PO4, 1.2 g/L Na2HPO4, 0.72 g/L glutamic acid, pH 7.5), and stored as single use aliquots at -80°C. The *C. muridarum* MoPn and CM001[75] and CM006-GFP strains were propagated in Vero cells and harvested by water lysis and sonication at 36 - 40 h post-infection.

Murine infection models

All animal experiments were approved and performed in accordance with the Duke University Institutional Animal Care and Use Committee. Animals were housed in a specific pathogen free environment with unrestricted access to food and water. Six-week-old female C57BL/6J mice (Jackson Laboratory, No. 000664) or 6-8 week old female *Eps8* transgenic age-matched littermates (derivation described below) were injected subcutaneously with 2.5 mg medroxyprogesterone (TEVA Pharmaceuticals) to synchronize their estrous cycles one week prior to infections. Intravaginal infections were performed with 1 x 10^6 – 1 x 10^7 mCherry-expressing *C. muridarum* (CM001), MoPn, or *tepP* mutant EBs. Transcervical infections were performed with 1 x 10^7 CTL2 or *tepP* mutant EBs or 5 x 10^5 *C. muridarum* MoPn or *tepP* mutant EBs per mouse using an NSET Embryo Transfer device (ParaTechs).

Organoid and stromal cell isolation from the mouse endometrium

Epithelial organoids and primary stromal fibroblasts were cultured as previously described.[7] Uterine horns from 6 – 12 week old female C57BL/6J (Jackson Labs, No. 000664) or *Eps8* littermates were isolated, washed in cold phosphate buffered saline (PBS; Gibco), cleared of adipose tissue, cut into ~ 2 mm pieces, and incubated in DMEM (Gibco) containing 0.2% collagenase A (Thermo Fisher Scientific), 10% FBS and 1 U/mL penicillin/streptomycin (Gibco) for 2.5 h at 37°C. The tissue pieces were subsequently rinsed three times with PBS, shaken vigorously with 12 mL of PBS containing 0.1% bovine serum albumin (BSA; Equitech Bio), and passed through a 70 μm strainer (Falcon); the flow through contained the stromal cell population. The previous step was repeated prior to inverting the filter over a 50 mL tube and the epithelial glands were recovered by passing 20 mL PBS containing 0.1% BSA. Fractions containing stromal cells and epithelial glands were centrifuged at 600 *g* for 5 min at 10°C. The stromal cells were resuspended in 2-3 mL of 50% L-WRN conditioned media containing 50 μg/mL gentamicin (Gibco) and plated in a 24 well plate (0.5 mL per well). Epithelial glands were resuspended ice cold growth factor reduced Matrigel (Corning) before adding DMEM/F12 (Gibco) at a 1:1 final ratio. Cell suspensions were plated as follows - 35 μL drops per well in a 24 well plate or 125 μL drop in a 35 mm dish (Cellvis) - and incubated at 37°C at 5% CO2 for 40 min before overlaying 50% L-WRN conditioned media in DMEM/F12 containing 50 μg/mL gentamicin (Gibco) and 50 ng/mL EGF (StemCell Technologies).

Generation of *Eps8* knockout mice

Targeted *Eps8* (ENSMUST00000058210.12) editing in C57BL/6 (Jackson Labs, No. 000664) mice was performed as follows: guide RNAs were designed using the CRISPOR algorithm.[76] High quality guides flanking *Eps8* exon 4 (sgRNA3: 5' CTGAGTTTCGTTACCTACTATGG 3' and sgRNA4: 5' TTACTGTTCAAGCGCTTAACTGG 3') were synthesized by in vitro transcription and screened via Guide-It screening (Clonetech). The CRISPR/Cas9 ribonucleotide complex containing 16 μM Cas9 (IDT Cat No. 1081059) and 0.4 μg/μL of each sgRNA was generated in RNP buffer containing 100 mM HEPES pH 7.5, 750 mM KCl, 5 mM MgCl2, 20 mM Tris (2-carboxyethyl) phosphine hydrochloride (TCEP; Sigma-Aldrich, cat. no. C4706), and 50% glycerol.[77] The complex was incubated at 37°C for 15 min prior to direct embryo electroporation using the Nepagene NEPA21 Type II electroporator with the CUY501P1-1.5 electrode with the following settings: Poring Pulse 40V; Length 3.5 ms; Interval 50 ms, No 4; D.Rate% 10; Polarity + and a Transfer Pulse 7V; Length 50ms; Interval 50 ms; No. 5; D.Rate% 40; Polarity +/-. The *Eps8* mutant founders were backcrossed twice to the C57BL/6 (Jackson Laboratory; No.00064). Genotyping was performed from mouse tail cuts digested in ~150 μL buffer containing 50 mM Tris pH 8.0, 100 mM NaCl, 10 mM EDTA, 0.5% Triton X-100, and proteinase K at 55°C for 4 h, heat-inactivated at 95°C for 10 min, and centrifuged at 12,000 *g* for 2 min. PCR analysis of the *Eps8* locus was performed with 1 μL of the tail digestion using the primers: 5'-ATTTATTCTACTATAGCTGACGTC-3' and 5'-TAGAGGGAGGAGGATTCA TAGTTC-3'. Founder mutants were backcrossed twice with C57BL/6J (Jackson Labs, No. 000664) and disruption of EPS8 expression was determined by western blot as detailed below.

METHOD DETAILS

Insertional mutagenesis of CTL0063 (*tmeA*), CTL0064 (*tmeB*), and *C. muridarum* TC0268 (*tepP*)

The CTL0063 and CTL0064 and *C. muridarum* TC0268 sequences were analyzed for target insertion sites using the TargeTron™ algorithm (Sigma-Aldrich). The primers for CTL0063: IBS(5'-AAAAAAGCTTATAATTATCCTTACTCAACCTATTGGTGCGCCCA GATAGGGTG-3'), EBS1d (5'-CAGATTGTACAAATGTGGTGATAACAGATAAGTCCTATTGTCTAACTTACCTTTCTTTGT-3'), EBS2

(TGAACGCAAGTTTCTAATTTCGGTTTTGAGTCGATAGAGGAAAGTGTCT), and the primers for CTL0064: IBS(5'-AAAAAAGCTTATA ATTATCCTTACTTCACTGACCCGTGCGCCCA GATAGGGTG-3'), EBS1d (5'-CAGATTGTACAAATGTGGTGATAACAGATAAGTCT GACCCCTT AACTTACCTTTCTTTGT-3'), EBS2 (5'-TGAACGCAAGTTTCTAATTTCGGTTTGAAGTCGATAG AGGAAAGTGTCT-3') were used with the EBS Universal Primer (Sigma-Aldrich) to retarget the pDFTT3::*aadA* plasmid[69] according to the TargeTron™ manual. The primers for TC0268: IBS (5'-AAAAAAGCTTATAATTATCCTTAGCTACCGCCTACGTGCGCCCAGATAGG GTG-3'), EBS1d (5'- CAGATTGTACAAATGTGGTGATAACAGATAAGTCGCCTACTCTAACTT ACCTTTCTTTGT-3'), and EBS2 (5'- TGAACG CAAGTTTCTAATTTCGATTGTAGCTCGATAG AGGAAAGTGTCT-3') were used with the EBS Universal Primer to retarget the pDFTT3::bla plasmid as above. The vectors were transformed into *E. coli* DH5α (Invitrogen) and clones were isolated and sequenced (Eton Bioscience) using the T7-promoter primer. CTL2 was transformed with each plasmid as follows: 1 x 10^8 IFU were incubated with 10 μg DNA in buffer containing 0.9 mM calcium chloride for 30 min at 25°C and added to a confluent monolayer of Vero cells in a six well plate, centrifuged at 1,500 *g* for 30 min at 10°C. At 12 h post-infection, 150 μg/mL spectinomycin (Millipore) was added. The infections were passaged every 44 - 48 h. Insertions were verified by PCR analysis of the spectinomycin cassette using the primers: *aadA* forward (5'-GTAACGCGTCCCGGGCCTGATAGTTTGGCTGTGAG-3') and *aadA* reverse (5'-TCTACGCGTTGCCT GACGATGCGTGGAG-3') and the junction spanning the *Chlamydia* DNA and the intronic insertion using the primers: CTL0063 sense (5'- ATGAGTATTCGACCTAC -3') and CTL0064 antisense (5'- ACTTCGAACACGCAATGCATC-3') with the TargeTron universal primer (Sigma-Aldrich). *C. muridarum* MoPn transformations were performed as above except that 1 x 10^7 IFU were used in the transformation reaction and EBs were harvested and passaged every 36 h post-infection. Transformants were verified by PCR analysis using primers targeting full-length *tepP* (5'- GGTACCCGTCGTGTTGTCTAAGTCTC-3') and (5'- GCGGCCGCTTATTGATTATCTA GTTCC-), the junction spanning *Chlamydia* DNA (5'- ACTACCTGTATCAACCTCTGATAG) and the universal primer above, and the *bla* cassette used above. *C. muridarum* MoPn and *tepP* mutant was confirmed by whole-genome sequencing.

Chlamydia transformations with shuttle plasmid vectors

The *C. muridarum* CM001 strain was transformed with p2TK2spec-Nigg-mCherry[71] as follows: Approximately 10^7 IFU were incubated with 15 μg DNA in buffer containing 0.9 mM calcium chloride for 40 min, added to confluent Vero cells in a six well plate, and centrifuged at 1,500 *g* for 30 min at 10°C. At 15 h post-infection, 500 ug/mL spectinomycin was added. The infections were passaged every 36-40 hours until inclusions were present and fluorescent. Transformants were subsequently plaque-purified to obtain a clonal strain. The CTL0063 (*tmeA*) and the CTL0064 (*tmeB*) insertional mutants described above were transformed with the GFP-expressing *E.coli-Chlamydia* shuttle vector p2TK2[67] as previously described.[7] In brief, 1 x 10^8 IFU were incubated with 10 μg DNA in buffer containing 0.9 mM calcium chloride for 30 min at 25°C and added to a confluent monolayer of Vero cells in a six well plate, centrifuged at 1,500 *g* for 30 min at 10°C. At 12 h post-infection, 1 U/mL penicillin was added. The infections were passaged every 44 - 48 h until GFP-positive inclusions were present when the penicillin concentration was raised to 5 U/mL prior to plaque purification. Clonal isolates were verified using GFP expression and primers targeting the *bla* cassette (5'-CGATCTGTC TATTTCGTTCA-3') and (5'-CGGTATTATCCCGTATTGAC-3').

Chlamydia infections in HeLa cells and fibroblasts

HeLa and MEF cells were cultured No.1 glass coverslips (Bellco Glass) coated with 30 μg/mL Type I Collagen (Invitrogen) in 10 mM glacial acetic acid (Sigma-Aldrich) for 10 min at 25°C. Coverslips and filters were rinsed once with media to remove excess acetic acid. The indicated *Chlamydia* strain (MOI=20) was diluted in the cold medium, vortexed for 15 s, and centrifuged onto cells at 1,500 *g* for 10-20 min at 10°C. The cells were replenished with warm media and incubated at 37°C for the indicated time. To depolymerize actin filaments after invasion, cells were infected for one hour prior to the addition of 1 μM Latrunculin A (Sigma-Aldrich) for 1 h.

A2EN polarization, infections, transepithelial electrical resistance (TEER), and live-cell imaging of cell dispersion

A2EN cells were polarized on either No. 1 glass coverslips (Bellco Glass) or polycarbonate or polyester transwell filters (0.4 μm pore; Corning) coated with Type I Collagen as above. A2EN cells (250-350k per coverslips or transwell filter) were cultured for 4-5 days in media containing 2 mM $CaCl_2$ prior to infections, infected (MOI=50) by centrifugation at 500 *g* for 5 min at 25°C, and replenished with warm media. TEER measurements were performed at the indicated timepoints using an Epithelial Volt/Ohm Meter (World Precision Instruments). TEER was calculated by subtracting TEER measurement from a blank filter in media and multiplying the resistance (Ohm) measurement by the filter area.

For the dual invasion assay in Figure 6, A2EN cells were infected as above with GFP-expressing CTL2 or *tepP* mutants (polarized MOI = 50; nonpolarized = 10). After 1.5 h, the mCherry-expressing M923 (*incA*) mutant (polarized MOI = 10; nonpolarized = 10) was added directly to the media. The infection proceeded for an additional 16-18 h. Cells were fixed with 3% paraformaldehyde for 20 min, rinsed five times with PBS, mounted on coverslides with FluorSave (EMD Millipore) mounting medium, and imaged on the Nikon widefield microscopy described below. For live cell imaging, 35 mm glass bottom dishes (Mat-Tek) were coated with collagen as above prior to plating 1.0 x 10^6 – 1.5 x 10^6 A2EN cells. Brightfield microscopy was performed on an inverted Zeiss AxioObserver Z.1 microscope equipped with a motorized stage, XCite 120XL metal halide light source, and a Pecon XL S1 incubator. Images were acquired using a Plan Apo DICII 20x/0.80 NA objective (Olympus) and an EM-CCD camera (Photometrics) every three minutes for 14 h at 37°C.

Please cite this article in press as: Dolat et al., *Chlamydia* repurposes the actin-binding protein EPS8 to disassemble epithelial tight junctions and promote infection, Cell Host & Microbe (2022), https://doi.org/10.1016/j.chom.2022.10.013

Endometrial organoid infections

Endometrial organoids were microinjected using an Eppendorf FemtoJet 4x coupled with a Stereo Microscope (Nikon). *C. trachomatis* CTL2 was diluted in PBS to a final concentration of 5 x 10^5 - 5 x 10^6 IFU/mL, vortexed for 30 s, and ~5 μL was pipetted into a glass capillary (Sutter Instrument Company) using a microloader tip (Eppendorf). The glass capillary tip was broken off and the organoids were punctured once using a steep vertical angle and injected with equal volumes. When co-injected with fluorescent dextran, *C. trachomatis* CTL2 was diluted in PBS containing 0.01 mg/mL 3kD Texas-Red dextran (Invitrogen). Live imaging was performed on the Nikon Ti2 described below using a humidified Okolab environmental chamber set to 37°C.

MDCK infections, transfections, and TEER

MDCK cells were plated on collagen-coated coverslips as above. Non-polarized and polarized cells – either 4 x 10^4 or 1.2 x 10^5 per coverslip – were cultured for two days, infected with CTL2-GFP (MOI = 10) by centrifugation at 500 *g* for 10 min at 25°C, and refed with warm media. Note that non-polarized cells achieved polarity in two days. At 18 - 20 h post-infection, cells were rinsed twice with warm PBS, fixed with 3% PFA in PBS for 20 min, and quenched with 0.25% ammonium chloride for 5 min. TEER measurements were performed as described above in 7.5 x 10^4 cells cultured on collagen-coated polycarbonate filters. Transfections were performed using jetPRIME reagents (PolyPlus) with 1,500 ng of the indicated vector, and cells were cultured for two days prior to infections (MOI=10) and/or fixation.

CRISPR design, targeting and generation of knockout cell lines

Gene edits in HeLa and A2EN cells using the CRISPR/Cas9 system in cells stably expressing Cas9 as generated by transduction with the lentiCas9-Blast (Addgene, #52962) using 100 μg/mL Blasticidin (Sigma-Aldrich) selection. Virus was produced in HEK293T cells by co-transfecting using the jetPRIME system (Polyplus) containing a single guide RNA (sgRNA) in a lentiGuide-Puro vector (Addgene, #52962), and a psPAX2 (Addgene; #12260) and pMD2.G (Addgene; #12259). The following sgRNA was used to target *EPS8*: TCATCTCTTCCAGTGTGATG. Cells were infected with virus particles in media containing 8 ug/mL polybrene for two days prior to selection with 1 μg/mL puromycin (Sigma-Aldrich) for two days and subsequent passaging in 10 μg/mL puromycin for two weeks. Single clones were isolated by limiting dilution in 96 well plates. Knockout efficiency was assessed by western blot analysis as described below.

Plasmids, primers, mutagenesis, and transfections

To generate C1-mCherry-TepP, the TepP ORF was PCR amplified from genomic DNA using primers 5'-TCTCGAGCTCAAATGAG CATCGGGGGAGTACG-3' and 5'- GGTGGATCCTTATTCCCTATCGA

CTTCTCTATC-3' and the Sac1 and BamH1 restriction sites. EGFP-EPS8 was a gift from Dr. Matthew Tyska (Vanderbilt University). The four tyrosine residues in EPS8 were sequentially mutated to phenylalanine using the NEB Q5 site-direct mutagenesis kit (New England Biolabs) according to the manufacturer's protocol using the following primers: Y525 5'-TGTTTTGAGTGGTTCAAAATTTCTA TCTATATGGCGATTAGAAGTTGG-3'and 5'-CCAACTTCTAATCGCCATATAGATAGAAA TTTTGAACCACTCAAAACA-3'; Y540 5'-C CTTGCTACAAAGTCAAACTTGGATTTGGCATATT TCTTGG-3' and 5'-CCAAGAAATATGCCAAATCCAAGTTTGACTTTGTAGCAA GG-3'; Y602

5'-TCTGTATAGTATGAGTAAAAGGTGGATCAGCACGCC-3' and 5'-GGCGTGCTGATC CACCTTTTACTCATACTATACAGA-3'; Y774 5'-GTACAGTGATTTGGCTAAAGACTCTC GCCCCTTCA-3' and 5'-TGAAGGGGCGAGAGTCTTTAGCCAAATCACTGTAC-3'. Clonal isolates were sequenced to verify each mutation. The EGFP-EPS8 truncation mutants were generated using the In-Fusion Snap Assembly Kit (Takara Bio) according to the manufacturer's protocol. The EGFP-EPS8-ΔABD (nt 1-1944) used primers: 5'-TCTCGAGCTCAAGCTATGAATGGTCATATTTCTAATCATCCC-3' and 5'-CCGCGGTACCGTCGATTATGACACAGGAACAGGTG CTG-3', and the EGFP-EPS8-SH3/ABD (1593-2469) use primers: 5'-TCTCGAGCTCAAGCTATGCAACCCAAGAAATATGCCAA ATC-3' and 5'-CCGCGGTACCGTCGATTAGTGACTGCTTCCTTCATCA-3'. The reactions were transformed into *E. coli* Stellar cells and clonal isolates were sequenced. Transfections were performed using jetPRIME (PolyPlus) reagents according to the manufacturer. HeLa and MEFs cells (5 x 10^4) were cultured on coverslips or 35 mm glass bottom dishes coated with collagen as above and transfected with 500 ng of the indicated plasmid for 24 – 48 h. In Figure S2, MEFs were incubated 1 μM Latrunculin A (Sigma-Aldrich) for 1 h.

Time-lapse spinning disk microscopy

All cell lines were cultured on collagen-coated 35 mm glass bottom dishes (Cellvis) as described above. HeLa cells expressing EGFP-EPS8 or *Eps8* -/- MEFs complemented with EGFP-EPS8 were infected with CTL2-mCherry (MOI = 50) for 1 h prior to imaging on an inverted Zeiss AxioObserver Z.1 microscope equipped with a motorized stage, XLIGHT V2 spinning disk unit (Crest Optics), and an Insert P environmental chamber (Zeiss). Images were acquired using a 60x/NA 1.4 objective (Olympus), an LDI multiline laser (89 North), a sCMOS ORCA Flash V3 camera (Hamamatsu), and the Metamorph software (Molecular Devices) every 15 s at 37°C. Live imaging of actin dynamics during infection was performed by first incubating polarized A2EN cells with 200 nM Sir-Actin (Cytoskeleton) for 1.5 h and subsequently infecting with GFP-expressing CTL2 (MOI=50) for 1 h prior to imaging on the same microscope using 0.5 μm slices every 30 s.

Please cite this article in press as: Dolat et al., *Chlamydia* repurposes the actin-binding protein EPS8 to disassemble epithelial tight junctions and promote infection, Cell Host & Microbe (2022), https://doi.org/10.1016/j.chom.2022.10.013

Determination of infectious progeny

Infectious units (IFU) were quantified using two 96 well plates of confluent cell lines indicated. The input IFU was assessed by counting inclusions at 24 h from infections of serial dilutions where the MOI < 1. In the second plate, the infection proceeded for 48 h (*C. trachomatis* CTL2) or 36 h (*C. muridarum*) and infectious units were recovered by rinsing cells once with water and incubating cells with water for 20 min. Cell lysates were serially diluted and confluent Vero cells were infected by centrifugation 1,500 *g* for 20 min at 10°C. The number of inclusions were counted in dilutions where the MOI < 1. The number of infectious units from the full cycle was compared to the input IFU to determine the output IFU. Three independent replicates in three biological replicates were performed and IFU output to input was normalized to control cell line.

Phosphotyrosine profiling in *Chlamydia*-infected A2EN cells

A2EN cells (1.5 x 10^7) were cultured in 150 mm dish and, in triplicate, mock-infected or infected (MOI=50) with *tepP* mutants complemented with TepP (pTepP) or an empty vector (pVector)[26] in HBSS at 4°C for 1 h prior to adding warm media for 4 h. The cells were washed once with cold PBS and collected in cold PBS containing cOmplete protease inhibitors (Millipore), scraped and transferred to a 50 mL conical tube, centrifuged at 2,000 *g* for 5 min at 4°C. The supernatant was discarded and the pellet was resuspended in 1 mL cold PBS containing protease inhibitors and phosphatase inhibitors and centrifuged at 2,000 *g* for 5 min at 4°C to isolate unlysed cells. The supernatant was discarded and the pellet was frozen at -80C. Samples were thawed and incubated with 100 mM ammonium bicarbonate and 8M urea, probe sonicated three times for 5 s, and centrifuged at 12,000 *g* for 5 min at 4°C. 6.6 mg of each sample was removed and normalized to 8.31 mg/mL with 50 mM ammonium bicarbonate containing 8M urea. All samples were then reduced for 20 min at 80°C with 10 mM dithiolthreitol and alkylated for 40 min at room temperature with 22 mM iodoacetamide. Samples were then diluted 1.6M urea with 50 mM ammonium bicarbonate. Trypsin was added to a 1:50 ratio (enzyme to total protein) and allowed to proceed for 18 h at 37°C. Samples were then acidified with 0.2% TFA (pH 2.5) and subjected to C18 SPE cleanup (Sep-Pak, 50 mg bed). Following elution, all samples were then frozen and then lyophilized to dryness. 6.6 mg digested peptide for each sample was resuspended in 1.0 mL IAP Buffer (Cell Signaling Technology) by vortexing and brief bath sonication, and transferred to an aliquot of pY-1000 PTMScan enrichment beads (Cell Signaling Technology). IP was performed for two hours at 4°C using end-over-end mixing. After spinning to settle the beads and removing the supernatant, pTyr enrichment beads were washed with three aliquots of PBS, one aliquot of water, and then eluted with two 50 μl aliquots of 0.15% TFA in water, for approximately 10 minutes at room temperature. Eluates were combined and taken through a C18 STAGE tip desalting cleanup, and resulting peptides were dried via speedvac. Samples were then spiked with 100 fmol pre-digested Bovine alpha casein. Quantitative LC/MS/MS was performed on 4 μL of each phosphopeptide enriched sample, using a nanoAcquity UPLC system (Waters Corp) coupled to a Thermo QExactive Plus high-resolution accurate mass tandem mass spectrometer (Thermo) via a nanoelectrospray ionization source. Briefly, the sample was first trapped on a Symmetry C18 300 mm 180 mm trapping column (5 l/min at 99.9/0.1 v/v water/acetonitrile), after which the analytical separation was performed using a 1.7 um Acquity BEH130 C18 75 mm 250 mm column (Waters Corp.) using a 5-min hold at 3% acetonitrile with 0.1% formic acid and then a 90-min gradient of 3 to 30% acetonitrile with 0.1% formic acid at a flow rate of 400 nanoliters/minute (nL/min) with a column temperature of 55°C. Data collection on the QExactive Plus mass spectrometer was performed in a data-dependent acquisition (DDA) mode of acquisition with a r = 70,000 (@ m/z 200) full MS scan from m/z 375 – 1600 with a target AGC value of 1e6 ions followed by 10 MS/MS scans at r-17,500 (@ m/z 200) at a target AGC value of $5e^4$ ions. A 20s dynamic exclusion was employed to increase depth of coverage. The total analysis cycle time for each sample injection was approximately 2 h. Sample order of data collection was interwoven between conditions to minimize temporal bias. Following the 9 LC-MS/MS analyses, data was imported into Rosetta Elucidator v3.3 (Rosetta Biosoftware, Inc), and all LC-MS/MS runs were aligned based on the accurate mass and retention time of detected ions (“features”) which contained MS/MS spectra using PeakTeller algorithm (Elucidator) and intensity-scaled based on a robust mean (10%) normalization of the identified pY phosphopeptide features. The relative peptide abundance was calculated based on area-under-the-curve (AUC) of aligned features across all runs. The overall dataset had 23,849 quantified isotope (peptide) groups. Additionally, 124,764 MS/MS spectra were acquired for peptide sequencing by database searching. This MS/MS data was searched against a SwissProt_Human database and *Chlamydia* database which also contained a reversed-sequence “decoy” database for false positive rate determination as well as Casein_Bovine as a surrogate internal standard. Database searching was performed within Mascot Server (Matrix Science) and annotated at a Mascot ion tolerance of 20.0 which resulted in a peptide false discovery rate of 0.70%. Searching allowed variable M (oxidation, +16 Da), and STY (phosphorylation, +80 Da). Differential expression of phosphopeptides were analyzed in Excel (Microsoft) using a heteroscedastic unpaired, two-tailed t-test and Volcano plots were generated in R Studio. Gene ontology enrichment analysis was performed in gProfiler[78] to identify the over-represented biological processes within dataset comparisons. Pathways were plotted if they reached significant $p < 0.01$.

Immunoprecipitations

In Figures 2E and 2F, A2EN cells were mock-infected or infected with the indicated strain (MOI=100) for 1 h, rinsed twice with PBS, and transferred to an Eppendorf tube by scraping in buffer containing 50 mM Tris pH 7.4, 150 mM NaCl, 5 mM EDTA, 1% Triton X-100, 1 mM PMSF with fresh addition of Halt alkaline phosphatase inhibitor (Thermo Fisher Scientific) and cOmplete cocktail protease inhibitors (Millipore) according to the manufacturer. Lysates were rotated at 4°C for 20 min, sonicated for 10s, rotated for an additional 10 min at 4°C, and cleared by centrifugation at 9,600 *g* for 10 min at 4°C. Input samples were collected before the lysate was incubated with 5 μL anti-EPS8 (Abcam; 96144) overnight at 4°C with rotation. The next day, 300 μL magnetic Protein A beads

(Sigma-Aldrich) was rinsed five times with cold lysis buffer, resuspend in 150 μL lysis buffer, and 50 μL was added to each sample. The tubes were incubated with rotation at 4°C for 2.5 h, gently washed five times with lysis buffer, resuspended in Lamaelli buffer, and boiled for 10 min. In Figure 3G, EGFP-EPS8 was co-immunoprecipitated with TepP-mCherry using the GFP Trap system (ChromoTek). Six well plates were coated with 30 μg/mL Type I Collagen (Invitrogen) in 10 mM acetic acid for 10 min and rinsed once with media. 293T cells (6 x 10^5 per well) were co-transfected with the indicated plasmid (1 μg total DNA per well) using the jetPRIME transfection protocol (Polyplus) for 24 h. Cells were gently rinsed twice with PBS and collected in lysis buffer (50 mM Tris pH 7.5, 150 mM NaCl, 1 mM EDTA, 0.5% Igepal, 1 mM PMSF containing fresh Halt alkaline phosphatase (Thermo Fisher Scientific) and Complete Midi cocktail protease inhibitor (Millipore). Samples were sonicated for 10 s, incubated with rotation at 4°C for 30 min, and cleared by centrifugation at 9,600 *g* for 5 min at 4°C. The supernatant was collected and incubated with GFP Trap beads (25 μL slurry per sample), which were previously washed five times with 0.5 mL lysis buffer. The samples were incubated with rotation at 4°C for 1.5 h, washed three times with lysis buffer, resuspended in Lamaelli buffer, vortexed, and boiled for 10 min. Equal volumes were analyzed by SDS-PAGE and western blot as below, and probed using anti-GFP (Invitrogen, A11122; 1:2000), anti-DsRed (Clonetech, 632496; 1:2000) and anti-tubulin as below.

Western blots

In Figures 2E, 2F, and 4A, cells were cultured in a six well plate and mock-infected or infected with CTL2 (MOI=50) for 1 - 2 h, rinsed twice with PBS, transferred to an Eppendorf tube by scraping in buffer containing 50 mM Tris-HCl pH 7.5, 150 mM NaCl, 0.5% Triton X-100, 5 mM EDTA, 1 mM PMSF, Halt alkaline phosphatase inhibitor (Thermo Fisher Scientific) and Complete midi-cocktail protease inhibitors (Millipore). The cell solution was subsequently incubated on ice for 30 min after brief (10 s) sonication. The lysates were cleared by centrifugation at 9,600 *g* for 5 min at 4°C, diluted in Lamaelli buffer and boiled for 5 min. Equal volumes were resolved using a 10% SDS-PAGE gel, transferred to a nitrocellulose membrane for 1 h at 4°C, blocked with PBS containing 5% milk and 0.1% Tween-20 for 1 h at 25°C, and sequentially probed with anti-EPS8 (Abcam; 1:2,000), anti-phospho-Tyr (Cell Signaling Technologies; 1:2,000), anti-MOMP (Gift from Dr. Ken Fields; 1:1000), and anti-alpha-tubulin (Sigma-Aldrich; 1:5,000) diluted in 5% milk and 0.1% Tween-20. In Figure 5J, primary stromal cells were rinsed twice with PBS and transferred to an Eppendorf tube by scraping in buffer containing 50 mM Tris pH 8.0, 150 mM NaCl, 1 mM EDTA, 0.5% Triton X-100, 0.1% SDS, 1 mM PMSF and 1x cOmplete protease inhibitors (Millipore), sonicated for 10 s and incubate on ice for 30 min. The lysates were cleared by centrifugation at 9,600 *g* for 5 min at 4°C, diluted in Lamaelli buffer and boiled for 5 min. Equal volumes were resolved using a 10% SDS-PAGE gel, transferred to a nitrocellulose membrane for 1 h at 4C, blocked with PBS containing 5% milk and 0.1% Tween-20 for 1 h at 25°C, and sequentially probed with anti-EPS8 (BD Biosciences; 1:2,500) and anti-actin (Sigma-Aldrich; 1:5,000). In Figure S3, HeLa cells were cultured in six well plates and treated with DMSO or 10 μM PP2 (Abcam) for 2 h and infected with CTL2 (MOI=50) for 1 h in the presence of DMSO or 10 μM PP2. Cells were washed twice with PBS and collected in lysis buffer containing 50 mM Tris pH 7.4, 150 mM NaCl, 5 mM EDTA, 0.5% Triton X-100, 1 mM PMSF, 1x cOmplete protease inhibitor (Millipore) and Halt alkaline phosphatase inhibitors (Thermo Fisher Scientific), briefly sonicated, and incubated on ice for 30 min. Lysates were cleared by centrifugation at 9,600 *g* for 5 min at 4°C, diluted in Lamaelli buffer and boiled for 5 min. Equal volumes were analyzed by SDS-PAGE as above. The nitrocellulose membrane was blocked with PBS containing 5% milk and 0.1% Tween-20 for 1 h at 25°C, and sequentially probed with anti-phospho-tyrosine (Cell Signaling Technologies; 1:2,500), anti-EPS8 (Abcam; 1:2,000), anti-tubulin (Sigma; 1:5,000) and anti-HtrA (Gift from Dr. Wilhelmina Huston; 1:1,000). All membranes were probed with anti-rabbit or anti-mouse LI-COR secondary antibodies (1:10,000) conjugated to near-infrared dyes prior to scanning on an Odyssey LI-COR.

Antibodies

For immunofluorescence microscopy, the following antibodies were used: mouse anti-EPS8 (BD Bioscience 610143; 1:200), anti-phopsho-Tyr (Cell Signaling Technologies 9411S; 1:200), anti-MOMP (Santa Cruz 57678; 1:500), anti-*C.muridarum* LPS (Gift from D. Rockey; 1:100), and rabbit anti-ZO-1 (Cell Signaling Technologies D7D12; 1:200), anti-E-cadherin (Cell Signaling Technologies 24E10; 1:500), anti-Cap1 (Gift from A. Subtil; 1:250), anti-IncG (Gift from T. Hackstadt; 1:250), anti-TepP and anti-Slc1 (both generated and validated in Chen et al.[20]; 1:100 and 1:500, respectively). The following secondary antibodies were used: cross-adsorbed goat-anti-mouse (H+L) and goat-anti-rabbit (H+L) conjugated to Alexa-488 (A-11029; A-11008), Alexa-555 (A-21428; A21422), or Alexa-647 (A-21244; A-21236.) All secondary antibodies were diluted 1:1000, vortexed gently and centrifuged at 8,000 *g* for 1 min.

Immunofluorescence microscopy and inside-outside staining

Cells on coverslips were washed twice with warm PBS and incubated with warm PBS containing 3% formaldehyde (Electron Microscopy Services) for 20 minutes at 25°C. The samples were quenched with 0.25% ammonium chloride for 5 min, rinsed three times with PBS, permeabilized with PBS containing 0.1% tx-100 for 10 min, and incubated with 2% BSA for 20 min at 25°C. Primary antibodies were diluted in 2% BSA and incubated on cells for either 1.5 h at 25°C or overnight at 4°C, washed three times for 3 min with 2% BSA, and incubated with secondary antibodies diluted in 2% BSA for 1 h at 25°C. In Figure 3A, HeLa cells were permeabilized with 2% BSA containing 0.1% saponin for 30 min at 25°C, and antibodies were subsequently diluted in the same buffer and incubations were performed as described above. Organoids were fixed and stained as previously performed.[7] To assess bacterial entry (inside-outside), cells were infected with GFP-expressing CTL2 and mutant strains (MOI = 20) and fixed as above at 30 min post-infection but not permeabilized. Cells were blocked with 2% BSA for 20 min and labeled with anti-MOMP as above. In images where actin was visualized, cells were incubated with phalloidin (Acti-Stain 488 or 555, 1:500; Cytoskeleton) for the final 20 min of secondary

Please cite this article in press as: Dolat et al., *Chlamydia* repurposes the actin-binding protein EPS8 to disassemble epithelial tight junctions and promote infection, Cell Host & Microbe (2022), https://doi.org/10.1016/j.chom.2022.10.013

incubation. Cells nuclei were labeled with Hoechst for 10 min with 2 ng/mL Hoechst (Thermo Fisher Scientific). Cells were mounted on glass coverslides using Vectashield (Vector Laboratories; H-1000) or FluorSave Reagent (Millipore).

Airyscan confocal imaging was performed on a laser scanning microscope (LSM 880; Zeiss) equipped with a motorized stage, Airyscan detector (Hamamatsu), and diode (405 nm), argon ion (488 nm), double solid-state (561 nm), and helium-neon (633 nm) lasers. Images were acquired using a C-Apochromatic 40x/1.2NA water (Zeiss) or 60x/1.4 NA oil objective (Zeiss), 0.3 μm sections and deconvolved using automatic Airyscan Processing in the Zen Software (Zeiss). Widefield deconvolution imaging was performed on an inverted microscopy (Nikon Ti2) equipped with a motorized stage, ORCA-Flash 4.0 V2 sCMOS camera (Hamamatsu), LED light source (Sola Light Engine). Images were acquired using a Plan Apo 10x/0.45 NA (Nikon) or Plan Apo 60x/1.4 NA oil objective (Nikon) and deconvolved using in the Nikon Elements Software. In Figure S5E, MDCK cells were imaged using an EVOS FL Cell Imaging System (Thermo Fisher Scientific) equipped with 10x/0.3 NA objective and a CCD camera. All images were exported to ImageJ and Adobe Photoshop where only linear adjustments to intensity were done.

Transmission electron microscopy

A2EN^{Cas9} and A2EN *EPS8* KO cells were cultured in collagen-coated six well plates for four days. Cells were rinsed twice with Hank's Buffered Saline Solution and fixed with buffer containing 0.05% malachite green, 2.5% glutaraldehyde, 100 mM sodium cacodylate (pH 6.7) for two hours at 25C. Cells were washed four times for five min with 100 mM sodium cacodylate and stained with 0.8% K3Fe(CN)6 with 1% osmium tetroxide. The cells were rinsed four times for 5 min with 100 mM sodium cacodylate, stained with 1% tannic acid for 20 min, and washed once for 5 min with 100 mM sodium cacodylate and twice for 5 min with molecular grade distilled water. The cells were stained with 0.5% uranyl acetate overnight at 4C, washed five times for 5 min with molecular grade distilled water, dehydrated with a series of ethanol incubations, and embedded in resin and vertically cut. Ultrathin sections were post-stained with uranyl acetate and lead citrate. Images were acquired on a FEI Tecnai G^2 Twin electron microscope at 6500x magnification.

Image analysis

All analyses were performed in ImageJ.[73] Cell dispersion was quantified by fluorescent intensity segmentation of the F-actin signal. Binary masks were generated using the Minimum Error algorithm and the percent of area covered in each field of view was measured. The cell free area was determined by subtracting the area coverage from 100. Host cell entry (inside-outside) was quantified from maximum projections by encircling individual cells, identifying the number of GFP-positive EBs (total) and the MOMP-positive EBs (outside) using the find maxima algorithm in ImageJ. The number inside (MOMP-negative) was defined by subtracting the number outside (MOMP-positive) from the total number of EBs, which was divided by the number of total EBs to determine the percent inside. Recruitment of the host proteins (EPS8 and ZO-1) to nascent inclusions was performed in either maximum projections or 3D reconstructions by encircling individual cells and identifying the number of total EBs using the find maximum algorithm. Inclusions positive for either host protein was marked manually. To measure the impact of *Chlamydia* infection on individual cell morphology, cell aspect ratio was manually derived by using the line tool to measure the distance through the center of the cell and through the nucleus to define the length and the width.

Organoid size was determined by subtracting the background from brightfield images to reduce out of focus signal, generating a binary image and extracting the perimeter of each organoid. Epithelial cell height in the organoid was measured manually using the ImageJ line tool. In the dextran leakage assays, the fluorescent dextran intensity was segmented and the mean intensity profile over time was derived using z-axis profile function. To measure EPS8 and ZO-1 intensity in MDCK cells, the lateral membrane was sampled 2-3 times using a 5 micron line. The total intensity was measured and divided by the length of the line to derive intensity per micron. In the dual invasion assay, the number of mCherry-positive, secondary inclusions was quantified in background-subtracted images from ten fields of view using the find maxima algorithm. In Figure 7, inclusion size was measured by fluorescence intensity segmentation of the inclusion membrane protein using binary masks of Cap1. Each inclusion was highlighted, and the area was exported. The number of inclusions per mouse swab were imaged using the same EVOS FL Cell Imaging System and objective described above. Background-subtracted images were processed with the denoise algorithm to remove small outliers using the default settings and inclusion number was enumerated using the find maxima algorithm. All plots were generated in either Microsoft Excel or R Studio.

Quantification of bacterial burden in mice

To measure *C. muridarum* burden, mice were swabbed with 30 turns of a sterile polyester tipped applicator (Puritan), which was dipped in 0.5 mL SPG buffer and turned 30 times. Confluent Vero cells were infected with 25 μL or serial dilutions by centrifugation at 1,500 *g* for 10 min, cultured for 20 – 24 h and fixed with either ice cold methanol for 10 min or 3% formaldehyde (Electron Microscopy Services) in PBS for 20 min. Mice infected transcervically with *C. trachomatis* CTL2 were sacrificed at 2, 4 and 6 days post-infection, and the upper genital tracts were excised and trimmed of adipose tissue and immediately homogenized in 1.5 mL PBS. DNA was extracted using a DNeasy kit (Qiagen) from 100 μL of homogenate following procedures recommended by the manufacturers.

Histological analysis of the female reproductive tract

Semiquantitative histopathology grading was performed by a board-certified veterinary anatomic pathologist masked to the treatment group on the upper genital tract from tissue excised at 14 dpi, cleared of adipose tissue and fixed in 10% formalin for two

days at room temperature. The tissue was paraffin embedded, cut at 5 μm sections, and stained with hematoxylin and eosin. Sections were imaged on an Olympus BX51 microscope equipped with a DP70 digital camera (Olympus). Tissue was scored using the following numeric criteria: 0 = normal, 1 = rare foci, 2 = scattered aggregates (1-4) or mild diffuse, 3 = numerous aggregates (> 4) or moderate diffuse, 4 = severe diffuse infiltration or confluence. The genital tract from mice infected for 45 d was excised and imaged using an iPhone XR. Gross pathology, such as hydrometra and hydrosalpinx, which are characterized by fluid-filled sacs or enlargements, were counted.

RT-qPCR

Quantitative PCR was performed on an a StepOne Plus Real Time PCR Systems (Applied Biosystems) using Power UP SYBR Green (Thermo Fisher Scientific). Quantification of *C. trachomatis* 16S rRNA and mouse GAPDH were performed in triplicate and based on standard curves from dilutions of purified *C. trachomatis* L2 and mouse DNA. Mouse PCR targets and primers used were: GAPDH (5'-ACTGAGCAAGAGAGGCCCTA-3', 5'-TATGGGGGTCTGGGATGGAA-3'), and *C. trachomatis* PCR targets and primers used were: 16S rRNA (5'-GGAGGCTGCAGTCGAGAATCT-3', 5'-TTACAACCCTAGAGCCTTCATCACA-3')[68]

QUANTIFICATION AND STATISTICAL ANALYSIS

All datasets contain three independent replicates and were analyzed in R Studio for equal variance and normality using a Levene Test or Shapiro test, respectively. Normally distributed datasets were analyzed using an unpaired, two-tailed t-test. Datasets with unequal variance or distributions were analyzed using a Welch's t-test or a Mann Whitney U test. The indicated statistical test for each experiment can be found in the figure legends and was performed in either R Studio or Microsoft Excel.